Published in final edited form as:
Environ Mol Mutagen. 2009 October ; 50(8): 672–696. doi:10.1002/em.20532.

Nucleation capacity and presence of centrioles define a distinct category of centrosome abnormalities that induces multipolar mitoses in cancer cells

Michael J. Difilippantonio[1], **B. Michael Ghadimi**[1], **Tamara Howard**[2], **Jordi Camps**[1], **Quang Tri Nguyen**[1], **Douglas K. Ferris**[3], **Dan L. Sackett**[4], and **Thomas Ried**[1]

[1]Genetics Branch, Center for Cancer Research, NCI/NIH

[2]Department of Cell Biology and Physiology, University of New Mexico - Health Sciences Center

[3]SAIC, Basic Research Laboratory, FCRDC, NCI/NIH

[4]Laboratory of Integrative and Medical Biophysics, NICHD/NIH

Abstract

Analysis of centrosome number and structure has become one means of assessing the potential for aberrant chromosome segregation and aneuploidy in tumor cells. Centrosome amplification directly causes multipolar catastrophic mitoses in mouse embryonic fibroblasts (MEFs) deficient for the tumor suppressor genes *Brca1* or *Trp53*. We observed supernumerary centrosomes in cell lines established from aneuploid, but not from diploid, colorectal carcinomas, however, multipolar mitoses were never observed. This discrepancy prompted us to thoroughly characterize the centrosome abnormalities in these and other cancer cell lines with respect to both structure and function. The most striking result was that supernumerary centrosomes in aneuploid colorectal cancer cell lines were unable to nucleate microtubules despite the presence of γ-tubulin, pericentrin, PLK1 and AURKA. Analysis by scanning electron microscopy revealed that these supernumerary structures are devoid of centrioles, a result significantly different from observations in aneuploid pancreatic cancer cell lines and in *Trp53* or *Brca1* deficient MEFs. Thus, multipolar mitoses are dependent upon the ability of extra γ-tubulin containing structures to nucleate microtubules, and this correlated with the presence of centrioles. The assessment of centrosome function with respect to chromosome segregation must therefore take into consideration the presence of centrioles and the capacity to nucleate microtubules.

Keywords

Centrosome; aneuploidy; chromosome instability; gene expression

Significance

The patterns and mechanisms of chromosomal aberrations in hematologic malignancies and solid tumors are fundamentally different. The former is characterized by specific

Corresponding Author: Michael J. Difilippantonio, 50 South Drive, Rm 1408, Bethesda, MD 20892, Phone: 301-435-3991, Fax: 301-402-1204.

chromosome translocations, whose consequence is the activation of oncogenes. Most carcinomas, however, reveal variations in the nuclear DNA content. The observed genomic imbalances and gross variations in chromosome number can result from unequal chromosome segregation during mitotic cell division. It is therefore fundamental to elucidate mechanisms involved in distribution of the genome to daughter cells. Prior to cell division, the centrosome organizes microtubules and the mitotic spindle. Deciphering the consequences of alterations in centrosome number, structure and function is an important step towards understanding how a diploid genome is maintained. Although extra centrosomes have now been observed in carcinomas and were correlated with aneuploidy, a careful functional investigation of these structures and their role in generating chromosome imbalances may lead to the identification of distinct mechanistic pathways of genomic instability. Understanding these pathways will also be important in determining whether they are potential molecular targets of therapeutic intervention.

Introduction

Over a century ago Theodor Boveri coined the term centrosome to describe the sub-cellular structures originally observed by Van Beneden in 1876. He postulated that due to their role in cell division, deviation in number from the two centrosomes normally present in each cell could have dire consequences with respect to the partitioning of chromosomes into the daughter cells. Subsequent chromosome missegregation could result in the loss of tumor inhibiting, and the gain of tumor promoting, chromosomes and that this served as the genetic basis of malignant transformation [Boveri 1929]. The development of molecular cytogenetic techniques [Kallioniemi et al. 1992; Schröck et al. 1996], and their recent adaptation to higher resolution platforms including whole genome sequencing [Dufva 2009; Pettersson et al. 2009], has enabled the comprehensive characterization of chromosomal aberrations in cancer genomes. It has become clear through the use of these techniques that solid tumors originating in epithelial cells of different organs are characterized by a distribution of specific and distinct genomic imbalances, that whole chromosome gains and losses are early events in tumorigenesis [Ried et al. 1999] and that strong selection for these events may have a causative role in tumorigenesis. Accordingly, Boveri's hypothesis with respect to chromosome segregation errors and the role of centrosomes in this process has been revisited [Brinkley and Goepfert 1998; Pihan and Doxsey 1999; Pihan et al. 1998].

The centrosome is positioned in the cytoplasm adjacent to the nucleus and its duplication is concurrent with replication of the genome during S phase. At the beginning of M phase, the two centrosomes separate to opposite poles of the nucleus where they nucleate the formation of mitotic spindles containing α- and β-tubulin, many of which eventually connect to kinetochore proteins associated with the centromere of each chromosome. A dynamic interplay between the microtubules, mitotic kinesins, and cytokinesins is necessary for the coordinated separation of sister chromatids, their migration to opposite poles and generation of the cleavage furrow at the end of mitosis [Bowerman 2004; Brinkley 2001; Neef et al. 2006; Petronczki et al. 2007; Rogers et al. 2004; Stearns 2001].

Centrosomes consist of centrioles and the pericentriolar matrix (PCM). The centrioles contain a protein known as centrin while the PCM contains γ-tubulin, pericentrin (PCNT),

hGCP2, GCP3/HsSpc98 and AKAP450 among other proteins too numerous to list [Brinkley 2001; Stearns 2001; Alieva and Uzbekov 2008]. Two protein families shown to regulate centrosome duplication and/or separation are the polo-like kinases (e.g. PLK1) and aurora family kinases (e.g., AURKA) [Glover et al. 1995; Lane and Nigg 1996]. Overexpression of these proteins results in supernumerary centrosomes, while abrogating expression causes a failure of centrosome migration [Lane and Nigg 1996; Zhou et al. 1998]. The Cdk2-cyclin E (Cdk2-E) complex has been shown to regulate centrosome duplication in *Xenopus* cell extracts [Hinchcliffe et al. 1999]. A positive feedback loop between the Xenopus Plk1 protein (Plx1) and a downstream protein kinase target xPlkk1 has also been demonstrated [Erikson et al. 2004; Qian et al. 1998a; Qian et al. 1998b], implicating yet another phosphorylation pathway regulating the centrosome cycle.

We and others have previously demonstrated the presence of supernumerary centrosomes in primary tumors and tumor cell lines of different origins [Ghadimi et al. 2000; Lingle et al. 1998; Pihan et al. 1998]. These findings have been touted as proof that extra centrosomes can cause aneuploidy through their direct role in mis-segregation of chromosomes during mitosis. In only a very few instances, however, has this mechanism been proven by direct visualization of aberrant mitotic figures [Fukasawa et al. 1996; Xu et al. 1999]. In the present study we have identified differences with respect to the type of centrosome aberrations occurring in tumorigenesis. Our results suggest that the failure of certain centrosomes to nucleate microtubules and organize the mitotic spindle could be due to the absence of centrioles. This is the first report to our knowledge of γ-tubulin structures lacking nucleation capacity in mammalian cells.

Experimental Procedures

Cell lines and RNA Isolation

The following colorectal cancer cell lines were used in this study: DLD-1, HCT116, p53HCT116, SW48, and LoVo (near-diploid); SW480, SW837, HT-29, T84, Colo 201 for immunocytochemistry and nucleation assays. For gene expression analysis Colo 320DM, LS411N, SK-CO-1, NCI-H508, and NCI-H716 (aneuploid) were also utilized. The pancreatic tumor cell lines included AsPC-1, BxPC-3, Capan-1, Capan-2, CFPac-1, Hs766T, Mia PaCa-2, Panc-1, SU 86.86. All of the aforementioned cell lines were obtained from the ATCC (American Type Culture Collection) and cultured following their recommendations, except p53HCT116, a derivative of HCT116 with a homozygous disruption of *TP53* [Bunz et al. 1998], which was kindly provided by Dr. Curtis C. Harris of the National Cancer Institute, NIH. Control fibroblasts were cultured from human foreskin. p53−/− mouse embryonic fibroblasts (MEFs) were obtained from Andre Nussenzweig of the National Cancer Institute, NIH.

RNA was extracted from the cell lines and primary tumors [Camps et al. In Press] following standard procedures (http://www.riedlab.nci.nih.gov/protocols.asp). Nucleic acid quantification was determined using the Nanodrop ND-1000 UV-VIS spectrophotometer (Nanodrop, Rockland, DE) and RNA quality was assessed using the Bioanalyzer 2100 (Agilent Technologies, Santa Clara, CA). Normal colon RNA isolated post-mortem from

five different donors without a history of colorectal cancer was purchased from Ambion (Applied Biosystems, Foster City, CA).

Antibodies

Mouse monoclonal antibodies were used to detect γ-tubulin (Sigma-Aldrich, St Louis, MO, T6557; diluted 1:2000) and α-tubulin (Sigma-Aldrich, T9026; diluted 1:1000). Anti-PCNT rabbit polyclonal antibodies were obtained from Berkley Ab Company, Berkley, CA (PRB-432C; diluted 1:100). Anti-PLK1 and anti-AURKA rabbit polyclonal antibodies were produced by injection of peptide [Hamanaka et al. 1995]. Secondary antibodies used for immunocytochemistry were purchased from Vector Laboratories, Burlingame, CA (Goat anti-rabbit-TR, TI-1000, diluted 1:1000) and Boehringer Mannheim, Indianapolis, IN (Goat anti-mouse-FITC, diluted 1:200).

Immunocytochemistry

Cells were grown on Falcon chamber slides (Becton & Dickinson, Bedford, MA), rinsed once each in PBS and PHEM buffer [PIPES (60mM), HEPES (25mM), EGTA (10mM), $MgCl_2$ (2mM), pH 6.9], fixed in ice cold methanol for 10 min and washed 4× with PBS. Slides were blocked with 5% normal goat serum (NGS), 1% BSA in PBS for 30 min at 37°C. Primary antibodies were diluted (as indicated above) in 1% NGS, 1% BSA in PBS and incubated for 45 min at 37°C followed by three washes in PBS. The primary antibodies were detected with Goat-anti-rabbit-TR and Goat anti-mouse-FITC followed by three washes in PBS. Cells were counterstained with DAPI and mounted with antifade [p-phenylene-diamine (5.52mM), 77% glycerol, 0.1×PBS, to pH 8.0 with carbonate/bicarbonate buffer (pH 9.0)]. Images were acquired using Leica Q-FISH software (Leica Imaging Systems, Cambridge, UK). A minimum of 50 mitotic figures and 300 interphase nuclei were evaluated for centrosome number and organization.

Nucleation Assays

Cell lines were grown on Falcon culture slides (Becton & Dickinson). Cells were then incubated with the microtubule destabilizing drug nocodazole (10 μg/ml) for 1.5 hour at 37°C, and washed two times with PBS at room temperature and allowed to recover by incubation in media for 5 – 10 min. Slides were then rinsed once in PBS, once with PHEM buffer and then fixed in −20°C methanol. Tubulin structures were detected by incubating cells with a monoclonal α-tubulin (Sigma-Aldrich, 1:1000) and rabbit polyclonal γ-tubulin (Sigma-Aldrich, 1:2000) antibodies for 45 min. Following three PBS washes, the primary antibodies were detected with a FITC labeled goat anti-mouse and a TRITC labeled goat anti-rabbit antibody (Sigma-Aldrich, 1:200 each) for 45 min and cells were counterstained with DAPI.

Standard Transmission Electron Microscopy and Immunoelectron Microscopy

Cultured cells were processed *in situ* and embedded for electron microscopy as described [Gonda et al. 1976]. Briefly, cells were cultured in a T-75 flask, rinsed once with PBS and fixed with sodium cacodylate buffer (0.1M, pH 7.2) [Electron Microscope Sciences, Fort Washington, PA] containing 2% glutaraldehyde [Tousimis, Rockville, MD] for 1 hr at room

temperature. The fixed cells were then rinsed with cacodylate buffer followed by post-fixation in cacodylate buffer + 1% osmium tetroxide [Electron Microscope Sciences, Fort Washington, PA] for 1 hr. The cells were dehydrated in an ethanol series (35%, 50%, 70%, 95%, and 100%) with three changes of absolute ethanol, embedded in pure Embed-812 epoxy resin [Electron Microscope Sciences, Fort Washington, PA] overnight and allowed to cure for 48 hrs at 55°C. Ultra thin-sections were cut and mounted on copper grids and stained with uranyl acetate followed by lead citrate. The sections were observed and photographed using a Hitachi H-7000 transmission electron microscope [Nissei Sanyo America, Ltd, Pleasanton, CA] operated at 75 kV.

For ICC/EM, cells were cultured on gridded glass coverslips (22×22 mm^2) (Bellco Biotechnology, Vineland, NJ) and washed in PBS. The cells were fixed in cytoskeletal buffer (CSK) [PIPES (910mM), NaCl (100mM), Sucrose (300mM), EGTA (1mM), $MgCl_2$ (3mM)] + 0.1% Triton X-100 for 30 min, CSK + 0.1% Triton X-100 + 1% glutaraldehyde for 2 min and CSK + 0.1% glutaraldehyde for 10 min. This was followed by two 15 min treatments with 0.1% $NaBH_4$ in PBS. The coverslips were then processed for immunofluorescence as stated above using mouse mAb against γ-tubulin detected with goat anti-mouse-FITC and counterstained with DAPI. Images were acquired of cells with aberrant numbers of γ-tubulin staining bodies using a Nikon FXA fluorescence microscope and their coordinates recorded. The coverslips were floated off the slides and washed several times in PBS and then immersed in PBS overnight at 4°C. The cells were then washed 2 × 5 min in PBS and followed by 3 × 5 min washes in 0.1M sodium cacodylate buffer (pH 7.0). Cells were post fixed in 1% osmium potassium ferrocyanide for 1 hour at room temperature, washed 2 × 5 min in 0.1M sodium cacodylate and then 2 × 5 min in dH_2O. Samples were stained with 2% aqueous uranyl acetate for 30 min. at room temp, washed 3 × 5 min in dH_20, dehydrated in ethanol and infiltrated and embedded in Epon/Araldite. Thin sections were cut, cells relocated by their coordinates and examined using a Hitachi H-7000 transmission electron microscope [Nissei Sanyo America, Ltd, Pleasanton, CA] operated at 75 kV.

Gene Expression Microarrays and Data Analysis

The procedure followed for the hybridization and analysis of the gene expression arrays can be found elsewhere for the primary tumors [Camps et al. 2008] and the CRC cell lines (Camps et al., In Press). Briefly, one ug each of cell line or normal human colon RNA (Ambion, Austin, TX) and Universal Human Reference RNA (Stratagene) were amplified and labeled with Cy3 and Cy5, respectively, using a T7 RNA Polymerase (Low RNA Input Fluorescent Linear Amplification Kit, Agilent) according to the manufacturer's protocols, and hybridized to the 44K oligonucleotide-based Whole Human Genome Microarray G4112F (Agilent). Similarly, RNA from primary tumors and normal human colon were labeled with Cy3 and subjected to mono-channel hybridization onto 4×44K Whole Human Genome Microarray (G4112F, Agilent). Microarrays were washed and processed using an Agilent G2565BA scanner. Data were quality controled and extracted using Agilent Technologies' Feature Extraction (version 9.1).

The analyses of the microarray experiments were performed with in-house developed software based on R version 2.6.2 (http://www.R-project.org). Gene expression data was obtained from 44K or 4×44K Agilent dual-channel arrays. Median per feature was used to summarize data when two or three technical replicates were available. The data were normalized using Linear & Lowess procedure in Agilent's Feature Extraction software. Features for which signals were below background (as assessed by "gSurrogatedUsed" or "rSurrogatedUsed") were forced to NA (not a number). The median measurement was used when more than 1 measurement was available per feature (i.e. median-summarization by array using "ProbeName"). The final CRC cell line dataset contained 20 samples (15 cell lines, and 5 normal colon samples), and 40380 features.

Results

Numerical Aberrations

Diploid and aneuploid colorectal tumor cell lines show striking differences with respect to both centrosome number and structure [Ghadimi et al. 2000]. Despite the presence of supernumerary centrosomes in the aneuploid tumors, we fail to observe a potential consequence of centrosome amplification, i.e. multipolar mitoses. We therefore began a thorough functional and structural analysis of centrosomes in normal cultured foreskin fibroblast cells, diploid tumors, and aneuploid tumors with and without multipolar mitoses. Based upon these analyses we identified distinct differences in the number, size and localization of the centrosomes in these cell types.

Normal fibroblasts, as well as the diploid colorectal cell lines (HCT116, DLD1, SW48), contained 1–2 γ-tubulin positive staining bodies resulting in the formation of a normal bipolar mitosis (Figs. 1A & 1D). The aneuploid colorectal cell lines (HT29, SW837, SW480, Colo201, T84) each had a subpopulation of cells containing ≥3 γ-tubulin positive bodies [Ghadimi et al. 2000], the size and morphology of which was variable (Fig. 1B: mononucleated or Fig. 1C: multinucleated cells). All of the observed mitoses were biplolar, however, with some exhibiting clusters of γ-tubulin at the poles (Fig. 2F). We therefore extended our analysis of centrosome defects to include aneuploid cancer cell lines of pancreatic origin. These lines also contained a percentage of cells with an abnormal number of γ-tubulin positive structures (Table I), however all were of equal size and morphology, a phenotype distinct from the colorectal cancer cell lines. In addition, we frequently observed multipolar mitoses (Fig. 2G).

Many of the aneuploid colorectal cancer cell lines contain inactivating *TP53* mutations. The pattern of interphase centrosome aberrations we observed was consistent with the centrosome amplification seen in *Trp53*−/− or *Brca1*−/− MEFs [Fukasawa et al. 1996; Xu et al. 1999]. This caused us to wonder whether *TP53* loss had a comparable consequence with respect to centrosome number in all cancer cell lines. In order to address this question, we took advantage of the diploid colorectal cancer cell line HCT116 made homozygously deficient for the *TP53* protein (p53HCT116) [Waldman et al. 1996]. Unlike the *TP53* wild-type parental cells, this cell line had centrosome amplification and multipolar mitoses akin to the *Trp53*−/− MEFs (see below).

Despite the absence of gross chromosome mis-segregation in the aneuploid colorectal cancer cell lines, we were interested in determining whether the interphase centrosome aberrations observed in the pancreatic cell lines could be directly correlated with events occurring during mitosis. A comparison of interphase and metaphase cell types in MiaPaCa2, Capan-2, CFPac-1, BxPC-3 and Capan-1 revealed that the percentage of interphase and metaphase cells with 1-2 centrosomes was similar (Fig. 2; Types 1I vs 1M). Thus, the population of interphase cells with normal centrosome numbers correlated with the percentage of metaphase cells containing two centrosomes and normal bi-polar mitotic spindles. This was not true, however, for HS766T, SU86.86, Panc-1 and AsPC-1 cells (Fig. 2).

Functional Aberrations

α-tubulin staining of mitotic spindles in *Brca1*−/− and *Trp53*−/− MEFs and in p53HCT116 and pancreatic cancer cell lines (Table 1 & [Sato et al. 2001]), revealed multiple nucleating centrosomes and multipolar mitosis, structures associated with gross chromosomal missegregation. Aberrant mitoses, however, were not observed in the aneuploid colorectal cell lines despite the presence of supernumerary γ-tubulin structures. This prompted us to assess whether all of the γ-tubulin structures in the aneuploid colorectal tumor cell lines were functionally capable of nucleating microtubules.

Nocodazole is a potent microtuble depolymerizing drug that causes cell cycle arrest at mitosis [Jordan et al. 1998]. The damage is reversible such that replacement with fresh medium allows repolymerization of the microtubules and the procession of mitosis. We therefore used nocodazole block and release to assess the ability of γ-tubulin structures to nucleate α-tubulin containing microtubules. Efficient microtubule nucleation from centrosomes was most readily observed in mitotic cells in the absence of nocodazole (Figs. 3A, D & G). The effectiveness of microtubule depolymerization by nocodazole can be seen in Figures 3B, E & H. In the diploid colorectal cell lines and normal fibroblasts (Fig. 3C), p53HCT116 (Fig. 3F), pancreatic cancer cell lines and p53−/− MEFs (data not shown), all γ-tubulin positive structures, regardless of their number, functioned as α-tubulin nucleating centers shortly after removal of nocodazole. This differed markedly from the aneuploid colorectal cancer cell lines in which, despite the presence of multiple γ-tubulin structures, only 1–2 centrosomes in each cell were observed to function as nucleating centers in the formation of normal mitotic spindles (Fig. 3I). Thus, the absence of multipolar mitoses in the aneuploid colorectal cancer cell lines correlated with the inability of supernumerary centrosomes to serve as nucleation centers for α-tubulin containing mitotic spindles.

Structural Aberrations

In an effort to determine why these supernumerary structures were not capable of giving rise to multipolar mitosis, co-localization studies of γ-tubulin with other centrosome-associated proteins were performed. PLK1 is normally associated with centrosomes throughout the cell cycle, until anaphase when it relocalizes to the metaphase plate and is distributed as two rings at the midbody during cytokinesis [Lane and Nigg 1996]. This pattern was recapitulated in both diploid (HCT116, p53HCT116, DLD1) and aneuploid (HT29, SW480, Colo201) CRC cell lines irrespective of the number of γ-tubulin positive structures. Representative images from different cell lines are shown in Figure 4A and 4B. In

interphase, AURKA is distributed in multiple, non-centrosomal nuclear foci. Its association with centrosomes only occurs during mitosis. This redistribution pattern was also recapitulated in all of the CRC cell lines analyzed (Figs. 4C–D), with AURKA localized to every γ-tubulin positive structure. PCNT, as part of the pericentriolar matrix (PCM), always co-localizes with γ-tubulin in centrosomes [Doxsey et al. 1994], as was the case in all of the analyzed cell lines (Figs. 4E-F). Thus, we found no difference in the centrosome-associated localization pattern of PLK1, AURKA or PCNT proteins between diploid and aneuploid colorectal tumor cell lines. The presence of these centrosome-associated proteins was therefore insufficient to nucleate mitotic spindles and generate multipolar mitoses.

Each centrosome, as visualized by electron microscopy, consists of a pair of centrioles oriented at 90° relative to one another. Both fibroblasts and the diploid CRC cell line DLD1 contained 1–2 centrosomes, each with a pair of appropriately oriented centrioles (Figs. 5A–C). Many of the *Trp53*−/− MEFs and p53HCT116 cells contained multiple centriole pairs, often found in clusters (Figs. 5D–F). This was not surprising given the normal association of PCNT, PLK1 and AURKA with all of the supernumerary γ-tubulin structures (Fig. 4) and the presence of multipolar mitoses in these cells (Fig. 3D & Fig.4F). Examination of the aneuploid colorectal cancer cell lines revealed the presence of only 1–2 centriole pairs in greater than 95% of the cells (Fig. 5G–I). In the remaining cells, clusters of centrioles were observed (Fig. 6L), however the perpendicular orientation between pairs of centrioles was sometimes lost (data not shown).

This differed from our previous immunocytochemical observation that 30 – 40% of the SW837 cells contained multiple γ-tubulin structures. We therefore grew the cells on gridded coverslips, performed immunocytochemistry, identified those cells with multiple γ-tubulin structures and recorded their coordinates. The cells were then embedded for electron microscopy, serial sections cut and the cells relocated based on their coordinates. This afforded us the opportunity to directly correlate the presence of γ-tubulin and centrioles. As anticipated, all of the supernumerary centrosomes in the *Trp53*−/− MEFs contained a perpendicularly oriented pair of centrioles (Fig. 6A–D). In the aneuploid SW837 cancer line, cells with multiple γ-tubulin structures were found to contain only one or two pairs of centrioles (Fig. 6E–H), despite analysis of serial sections through the cells. Cells containing clusters of centrioles (Fig. 6I–L) did not always aggregate all of their γ-tubulin in one location. Thus, we were greatly surprised to find that the supernumerary structures containing γ-tubulin, PCNT and PLK in the aneuploid colorectal cancer cell lines were actually devoid of centrioles, thereby correlating the presence of centrioles with the nucleation capacity of γ-tubulin structures and the propensity for catastrophic multipolar mitoses.

Gene Expression Analysis

One approach to query the large number of genes currently known to be involved in centrosome regulation and function is global gene expression analysis. We expanded our set of CRC cell lines to include an additional five aneuploid CRC cell lines as well as five biopsies of normal colon epithelia. These results were also compared to a previous analysis consisting of 23 primary colon carcinomas [Camps et al. In Press]. Of the 131 genes spotted

on the array that we queried based on their known or potential connection to the development of aneuploidy through an association with the centromere, centrosome or spindles, 11 genes were significantly deregulated (P<0.0001) in both the diploid and aneuploid cell lines relative to the mucosa, and of these seven were also of significance in primary colon tumors (Table 2). Only *CSSP1* (1.48–1.96-fold decrease, P=0.009–0.0005), *CETN2* (2.23-fold increase, P=0.000104), *TTL4* (1.4-fold increase, P=0.009) and *TUBGCP6* (1.52-fold decrease, P=0.0039) had an expression difference that reached any significance (P<0.01) in the aneuploid relative to the diploid cell lines.

Discussion

In an effort to understand the causal events leading to the development of aneuploidy in tumorigenesis, we have undertaken a comparative analysis of centrosomes and gene expression profiles in cultured normal foreskin fibriblasts, diploid and aneuploid tumor cell lines with and without multipolar mitoses. Most published reports of centrosome analysis in primary tumors and tumor cell lines address the number and morphology of these structures in interphase nuclei as visualized by immunocytochemistry with antibodies against γ-tubulin or PCNT. In addition to an examination of their presence and abundance in interphase nuclei, we also wanted to determine the manifestations of such aberrations in dividing cells and attempt to make a correlation between these two phases of the cell cycle (Figure 2). Our analysis included a categorization of interphase and metaphase cells into three distinct classes. Those we labeled as Type 2 and Type 3 corresponded to cells with an increase in centrosome number. According to Theodore Boveri, such cells might be expected to undergo aberrant chromosome segregation. This is in fact what we observed in the pancreatic cell lines, p53HCT116 and *Trp53*−/− MEFs. Whether the resulting daughter cells would be viable is an issue that can only truly be addressed by identifying the aberrant cells and following them through cell division.

The situation, however, was quite different in the CRC cancer cell lines. Defects in DNA mismatch repair pathway (MMR−/−) results in the accumulation of point mutations or small lesions throughout the genome, eventually occurring in tumor suppressor genes or oncogenes. Such genomic alteration abrogates the need for changes in chromosome copy number during tumorigenesis [Lengauer et al. 1998]. Consistent with this mechanism of mutagenesis, we found that these cells contain normal numbers of centrosomes, all of uniform size, shape and protein composition as determined by immunocytochemistry (ICC) against multiple centrosome-associated structural proteins and kinases. Their capacity to nucleate α-tubulin containing microtubules was similar to control fibroblast cells [Ghadimi et al. 2000] and each centrosome was found to contain two perpendicularly oriented centrioles.

The loss of TP53 function can induce true centrosome amplification in otherwise wildtype (*Trp53*−/− MEFSs) and MMR deficient cells (p53HCT116). The *TP53* deficient diploid CRC cell line DLD1, which contains only 1–2 normal centrosomes, provides evidence that there may be other factors that can counteract this predisposition. Our observations in the p53HCT116 cell line suggest that although TP53 loss can induce the amplification of

functional centrosomes and multipolar mitoses in MMR−/− cells, it did not result in an increase in chromosome instability (data not shown).

The aneuploid colorectal cancers contain an intact DNA mismatch repair pathway (MMR+), but generally have loss of TP53 function. As such, the accumulation of genomic alterations primarily occurs through their inability to correctly respond to certain types of DNA lesions. This includes a failure to arrest the cell cycle and to activate the repair pathways necessary for proper repair of the damaged DNA. Such cells are also capable of altering the number of intact oncogenes and tumor suppressor genes via the gain and loss of chromosomes or chromosomal regions [Eshleman et al. 1998]. One potential mechanism for altering chromosome copy number is interference with the chromosome segregation machinery. Consistent with this idea was the presence of multiple γ-tubulin structures in the aneuploid colorectal cells that presumably represented functional centrosomes. We have now demonstrated that these extra structures contain a number of microtubule organizing center (MTOC) proteins considered to be the hallmark of functional centrosomes (i.e., γ-tubulin and PCNT) [Doxsey et al. 1994; Moritz et al. 1995]. The co-localization pattern of these proteins, as well as the cell-cycle dependent co-localization and redistribution of two kinases known to be involved in centrosome segregation and migration (i.e., PLK1 and AURKA), were identical in aneuploid and diploid CRC cell lines and in normal cells.

Further examination, however, revealed that these supernumerary structures did not behave like centrosomes. The presence of multipolar mitosis in the *Brca1*−/− and *Tp53*−/− MEFs, p53HCT116 and pancreatic tumor cell lines, all of which contained multiple γ-tubulin structures, was in sharp contrast to observations in the aneuploid CRC cell lines. The inability of the structures in the latter lines to nucleate α-tubulin containing microtubules, as revealed in our nucleation assays, provides one explanation. This is somewhat surprising given evidence that γ-tubulin is responsible for the nucleation activity of centrosomes [Mogensen et al. 1997].

Our dual immunocytochemistry / EM analysis revealed the presence of only 1–2 pairs of centrioles in most of the aneuploid CRC cells despite the presence of multiple γ-tubulin structures. Even in SW837 where we observed multiple centrioles in an exceedingly low percentage of cells (Fig. 6I–L), we did not observe more than two clusters of centrioles per cell. Thus, there appears to be a clear correlation between nucleation ability and the presence of centrioles in the tumor cell lines analyzed here. This is in contrast to observations in early mouse development and certain *Drosophila* cell lines, where centrosomes stripped of their centrioles have been shown to have nucleation activity [Debec et al. 1995]. It is also possible that nucleation from these structures occurs but is severely impaired, hence the inability of it to be detected in our assay.

Perhaps modification of γ-tubulin is essential to its ability for nucleation [Khodjakov and Rieder 2001]. Our co-localization studies indicate that two proteins (PLK1 and AURKA) whose modification of γ-tubulin is critical for progression through the cell cycle are associated with, and therefore in a position to modify, γ-tubulin in these non-functional structures [Feng et al. 1999]. Our analysis here of CRC cell lines, as well as of primary colon tumors (data not shown), confirms the findings of previous studies demonstrating

elevated levels of these proteins in primary human colorectal cancers [Bischoff et al. 1998; Takahashi et al. 2000]. While the protein concentrations and localization may be sufficient for the modification of γ-tubulin in the aneuploid cells, their enzymatic activity was not assessed. Analysis of Xenopus extracts has identified Xmap215 as a protein which is critical for the nucleation of mitotic spindles [Popov et al. 2002]. Perhaps a failure of the human orthologous protein (CKAP5), which we observed to be significantly increased at the transcriptional level, to localize to the supernumerary, centriole-lacking structures is responsible for their inability to nucleate spindle formation.

Further molecular interrogation of the differentially expressed genes identified through our analysis will be necessary to determine if they are in any way related to the functional capacity of γ-tubulin containing structures to nucleate mitotic spindles and form multipolar mitoses capable of causing chromosome mis-segregation. Overexpression of CSPP1, as occurs in the aneuploid CRC cell lines, has been shown to result in a cell cycle block at M and early G1 phases, with mitosis-arrested cells containing aberrant spindles [Patzke et al. 2005]. CETN2 localizes to spindles [Salisbury 1995] and more recently has been found associated with the nuclear pore complex [Resendes et al. 2008] were it regulates mRNA and protein export into the cytoplasm. It has also been demonstrated to stimulate the early stages of nucleotide excision repair [Nishi et al. 2005] through its interaction with xeroderma pigmentosum group C protein (XPC1) [Popescu et al. 2003]. One of the γ-tubulin complex proteins, TUBGCP6, was expressed at lower levels in the aneuploid CRC cell lines. Because of its association with the γ-tubulin complex, a decrease in expression might explain the failure of the supernumerary structures in the CRC aneuploid cell lines to nucleate microtubules [Murphy et al. 2001].

Our results suggest the potential of antibodies against γ-tubulin or PCNT alone to be misleading, particularly when drawing inferences about the functionality of these structures. We have identified three distinct categories of tumor cells based on their centrosome number and functionality. The first contain a normal complement of functional centrosomes. This is exemplified by the near diploid colorectal tumors. The second consists of cells with supernumerary centrosomes that have nucleating capacity, thereby resulting in active chromosome mis-segregation via multipolar mitoses. These would include the pancreatic tumor cell lines, *Brca1* and *Tp53*-deficient MEFs, p53HCT116 and *Brca1*-deficient tumors [Weaver et al. 2002; Xu et al. 1999]. The degree of chromosomal instability in these cells may, however, depend on other factors such as the rate of mis-segregation and the fate of the daughter cells. The final series of cell lines, which includes the aneuploid colorectal cancer cell lines, have an abnormal distribution of centrosome-associated proteins, possibly through fragmentation of the pericentriolar matrix. Since the supernumerary structures were not capable of nucleating microtubules, and because multipolar mitoses were never observed, one might speculate that the consequence is an alteration of the functional capacity of "legitimate" centrosomes. As such, mis-segregation would result from a failure of sister chromatid separation rather than the active aberrant partitioning of chromosomes via attachment to the supernumerary centrosomes. Perhaps not surprisingly, these cell lines were no more karyotypically unstable than those cell lines containing a normal pair of centrosomes (data not shown).

In conclusion, the presence of γ-tubulin, pericentrin, and the modifying kinases PLK and AURKA are insufficient for the generation of a functional centrosome with the capacity to nucleate microtubules. Such supernumerary structures are therefore incapable of inducing the formation of multipolar mitoses, however we cannot exclude a possible role in chromosome mis-segregation through disruption of the normal bipolar spindle. The assessment of centrosome function with respect to chromosome segregation must therefore take into consideration the presence of centrioles and the capacity to nucleate microtubules.

Acknowledgements

The authors would like to thank Kunio Nagashima for help with the EM analysis, Cristina Montagna for her insightful suggestions, Andre Nussenzweig and Curtis Harris for generously providing cell lines, and David Spector for critical reading of the manuscript. Supported in part by the Intramural Research Program of the NIH, National Cancer Institute, Center for Cancer Research.

References

Alieva IB, Uzbekov RE. The centrosome is a polyfunctional multiprotein cell complex. Biochemistry (Mosc). 2008; 73(6):626–643. [PubMed: 18620528]

Bischoff JR, Anderson L, Zhu Y, Mossie K, Ng L, Souza B, Schryver B, Flanagan P, Clairvoyant F, Ginther C, et al. A homologue of Drosophila aurora kinase is oncogenic and amplified in human colorectal cancers. Embo J. 1998; 17(11):3052–3065. [PubMed: 9606188]

Boveri, T. The origin of malignant tumors. Baltimore: Williams & Wilkins; 1929.

Bowerman B. Cell division: timing the machine. Nature. 2004; 430(7002):840–842. [PubMed: 15318203]

Brinkley BR. Managing the centrosome numbers game: from chaos to stability in cancer cell division. Trends Cell Biol. 2001; 11(1):18–21. [PubMed: 11146294]

Brinkley BR, Goepfert TM. Supernumerary centrosomes and cancer: Boveri's hypothesis resurrected. Cell Motil Cytoskeleton. 1998; 41(4):281–288. [PubMed: 9858153]

Bunz F, Dutriaux A, Lengauer C, Waldman T, Zhou S, Brown JP, Sedivy JM, Kinzler KW, Vogelstein B. Requirement for p53 and p21 to sustain G2 arrest after DNA damage. Science. 1998; 282(5393): 1497–1501. [PubMed: 9822382]

Camps J, Grade M, Nguyen QT, Hormann P, Becker S, Hummon AB, Rodriguez V, Chandrasekharappa S, Chen Y, Difilippantonio MJ, et al. Chromosomal breakpoints in primary colon cancer cluster at sites of structural variants in the genome. Cancer Res. 2008; 68(5):1284–1295. [PubMed: 18316590]

Camps, J.; Nguyen, QT.; Padilla-Nash, HM.; Knutsen, T.; McNeil, NE.; Wangsa, D.; Hummon, AB.; Grade, M.; Ried, T.; Difilippantonio, MJ. Integrative Genomics Reveals Mechanisms of Copy Number Alterations Responsible for Transcriptional Deregulation in Colorectal Cancer. In Press

Debec A, Detraves C, Montmory C, Geraud G, Wright M. Polar organization of gamma-tubulin in acentriolar mitotic spindles of Drosophila melanogaster cells. J Cell Sci. 1995; 108(Pt 7):2645–2653. [PubMed: 7593305]

Doxsey SJ, Stein P, Evans L, Calarco PD, Kirschner M. Pericentrin, a highly conserved centrosome protein involved in microtubule organization. Cell. 1994; 76(4):639–650. [PubMed: 8124707]

Dufva M. Introduction to microarray technology. Methods Mol Biol. 2009; 529:1–22. [PubMed: 19381982]

Erikson E, Haystead TA, Qian YW, Maller JL. A feedback loop in the polo-like kinase activation pathway. J Biol Chem. 2004; 279(31):32219–32224. [PubMed: 15166215]

Eshleman JR, Casey G, Kochera ME, Sedwick WD, Swinler SE, Veigl ML, Willson JK, Schwartz S, Markowitz SD. Chromosome number and structure both are markedly stable in RER colorectal cancers and are not destabilized by mutation of p53. Oncogene. 1998; 17(6):719–725. [PubMed: 9715273]

Feng Y, Hodge DR, Palmieri G, Chase DL, Longo DL, Ferris DK. Association of polo-like kinase with alpha-, beta- and gamma-tubulins in a stable complex. Biochem J. 1999; 339(Pt 2):435–442. [PubMed: 10191277]

Fukasawa K, Choi T, Kuriyama R, Rulong S, Vande Woude GF. Abnormal centrosome amplification in the absence of p53. Science. 1996; 271(5256):1744–1747. [PubMed: 8596939]

Ghadimi BM, Sackett DL, Difilippantonio MJ, Schrock E, Neumann T, Jauho A, Auer G, Ried T. Centrosome amplification and instability occurs exclusively in aneuploid, but not in diploid colorectal cancer cell lines, and correlates with numerical chromosomal aberrations. Genes Chromosomes Cancer. 2000; 27(2):183–190. [PubMed: 10612807]

Glover DM, Leibowitz MH, McLean DA, Parry H. Mutations in aurora prevent centrosome separation leading to the formation of monopolar spindles. Cell. 1995; 81(1):95–105. [PubMed: 7720077]

Gonda MA, Aaronson SA, Ellmore N, Zeve VH, Nagashima K. Ultrastructural studies of surface features of human normal and tumor cells in tissue culture by scanning and transmission electron microscopy. J Natl Cancer Inst. 1976; 56(2):245–263. [PubMed: 1255758]

Hamanaka R, Smith MR, O'Connor PM, Maloid S, Mihalic K, Spivak JL, Longo DL, Ferris DK. Polo-like kinase is a cell cycle-regulated kinase activated during mitosis. J Biol Chem. 1995; 270(36): 21086–21091. [PubMed: 7673138]

Hinchcliffe EH, Li C, Thompson EA, Maller JL, Sluder G. Requirement of Cdk2-cyclin E activity for repeated centrosome reproduction in Xenopus egg extracts [see comments]. Science. 1999; 283(5403):851–854. [PubMed: 9933170]

Jordan A, Hadfield JA, Lawrence NJ, McGown AT. Tubulin as a target for anticancer drugs: agents which interact with the mitotic spindle. Med Res Rev. 1998; 18(4):259–296. [PubMed: 9664292]

Kallioniemi A, Kallioniemi OP, Sudar D, Rutovitz D, Gray JW, Waldman F, Pinkel D. Comparative genomic hybridization for molecular cytogenetic analysis of solid tumors. Science. 1992; 258:818–821. [PubMed: 1359641]

Khodjakov A, Rieder CL. Centrosomes enhance the fidelity of cytokinesis in vertebrates and are required for cell cycle progression. J Cell Biol. 2001; 153(1):237–242. [PubMed: 11285289]

Lane HA, Nigg EA. Antibody microinjection reveals an essential role for human polo-like kinase 1 (Plk1) in the functional maturation of mitotic centrosomes. Journal of Cell Biology. 1996; 135:1701–1713. [PubMed: 8991084]

Lengauer C, Kinzler KW, Vogelstein B. Genetic instabilities in human cancers. Nature. 1998; 396(6712):643–649. [PubMed: 9872311]

Lingle WL, Lutz WH, Ingle JN, Maihle NJ, Salisbury JL. Centrosome hypertrophy in human breast tumors: Implications for genomic stability and cell polarity. Proc.Natl.Acad.Sci.USA. 1998; 95:2950–2955. [PubMed: 9501196]

Mogensen MM, Mackie JB, Doxsey SJ, Stearns T, Tucker JB. Centrosomal deployment of gamma-tubulin and pericentrin: evidence for a microtubule-nucleating domain and a minus-end docking domain in certain mouse epithelial cells. Cell Motil Cytoskeleton. 1997; 36(3):276–290. [PubMed: 9067623]

Moritz M, Braunfeld MB, Sedat JW, Alberts B, Agard DA. Microtubule nucleation by gamma-tubulin-containing rings in the centrosome. Nature. 1995; 378(6557):638–640. [PubMed: 8524401]

Murphy SM, Preble AM, Patel UK, O'Connell KL, Dias DP, Moritz M, Agard D, Stults JT, Stearns T. GCP5 and GCP6: two new members of the human gamma-tubulin complex. Mol Biol Cell. 2001; 12(11):3340–3352. [PubMed: 11694571]

Neef R, Klein UR, Kopajtich R, Barr FA. Cooperation between mitotic kinesins controls the late stages of cytokinesis. Curr Biol. 2006; 16(3):301–307. [PubMed: 16461284]

Nishi R, Okuda Y, Watanabe E, Mori T, Iwai S, Masutani C, Sugasawa K, Hanaoka F. Centrin 2 stimulates nucleotide excision repair by interacting with xeroderma pigmentosum group C protein. Mol Cell Biol. 2005; 25(13):5664–5674. [PubMed: 15964821]

Patzke S, Hauge H, Sioud M, Finne EF, Sivertsen EA, Delabie J, Stokke T, Aasheim HC. Identification of a novel centrosome/microtubule-associated coiled-coil protein involved in cell-cycle progression and spindle organization. Oncogene. 2005; 24(7):1159–1173. [PubMed: 15580290]

Petronczki M, Glotzer M, Kraut N, Peters JM. Polo-like kinase 1 triggers the initiation of cytokinesis in human cells by promoting recruitment of the RhoGEF Ect2 to the central spindle. Dev Cell. 2007; 12(5):713–725. [PubMed: 17488623]

Pettersson E, Lundeberg J, Ahmadian A. Generations of sequencing technologies. Genomics. 2009; 93(2):105–111. [PubMed: 18992322]

Pihan GA, Doxsey SJ. The mitotic machinery as a source of genetic instability in cancer. Semin Cancer Biol. 1999; 9(4):289–302. [PubMed: 10448116]

Pihan GA, Purohit A, Wallace J, Knecht H, Woda B, Quesenberry P, Doxsey SJ. Centrosome defects and genetic instability in malignant tumors. Cancer Research. 1998; 58:3974–3985. [PubMed: 9731511]

Popescu A, Miron S, Blouquit Y, Duchambon P, Christova P, Craescu CT. Xeroderma pigmentosum group C protein possesses a high affinity binding site to human centrin 2 and calmodulin. J Biol Chem. 2003; 278(41):40252–40261. [PubMed: 12890685]

Popov AV, Severin F, Karsenti E. XMAP215 is required for the microtubule-nucleating activity of centrosomes. Curr Biol. 2002; 12(15):1326–1330. [PubMed: 12176362]

Qian YW, Erikson E, Li C, Maller JL. Activated polo-like kinase Plx1 is required at multiple points during mitosis in Xenopus laevis. Mol Cell Biol. 1998a; 18(7):4262–4271. [PubMed: 9632810]

Qian YW, Erikson E, Maller JL. Purification and cloning of a protein kinase that phosphorylates and activates the polo-like kinase Plx1. Science. 1998b; 282(5394):1701–1704. [PubMed: 9831560]

Resendes KK, Rasala BA, Forbes DJ. Centrin 2 localizes to the vertebrate nuclear pore and plays a role in mRNA and protein export. Mol Cell Biol. 2008; 28(5):1755–1769. [PubMed: 18172010]

Ried T, Heselmeyer-Haddad K, Blegen H, Schrock E, Auer G. Genomic changes defining the genesis, progression, and malignancy potential in solid human tumors: a phenotype/genotype correlation. Genes Chromosom Cancer. 1999; 25(3):195–204. [PubMed: 10379865]

Rogers GC, Rogers SL, Schwimmer TA, Ems-McClung SC, Walczak CE, Vale RD, Scholey JM, Sharp DJ. Two mitotic kinesins cooperate to drive sister chromatid separation during anaphase. Nature. 2004; 427(6972):364–370. [PubMed: 14681690]

Salisbury JL. Centrin, centrosomes, and mitotic spindle poles. Curr Opin Cell Biol. 1995; 7(1):39–45. [PubMed: 7755988]

Sato N, Mizumoto K, Nakamura M, Maehara N, Minamishima YA, Nishio S, Nagai E, Tanaka M. Correlation between centrosome abnormalities and chromosomal instability in human pancreatic cancer cells. Cancer Genet Cytogenet. 2001; 126(1):13–19. [PubMed: 11343773]

Schröck E, du Manoir S, Veldman T, Schoell B, Wienberg J, Ferguson-Smith MA, Ning Y, Ledbetter DH, Bar-Am I, Soenksen D, et al. Multicolor spectral karyotyping of human chromosomes. Science. 1996; 273(5274):494–497. [PubMed: 8662537]

Stearns T. Centrosome duplication. a centriolar pas de deux. Cell. 2001; 105(4):417–420. [PubMed: 11371338]

Takahashi T, Futamura M, Yoshimi N, Sano J, Katada M, Takagi Y, Kimura M, Yoshioka T, Okano Y, Saji S. Centrosomal kinases, HsAIRK1 and HsAIRK3, are overexpressed in primary colorectal cancers. Jpn J Cancer Res. 2000; 91(10):1007–1014. [PubMed: 11050471]

Waldman T, Lengauer C, Kinzler KW, Vogelstein B. Uncoupling of S phase and mitosis induced by anticancer agents in cells lacking p21. Nature. 1996; 381(6584):713–716. [PubMed: 8649519]

Weaver Z, Montagna C, Xu X, Howard T, Gadina M, Brodie SG, Deng CX, Ried T. Mammary tumors in mice conditionally mutant for Brca1 exhibit gross genomic instability and centrosome amplification yet display a recurring distribution of genomic imbalances that is similar to human breast cancer. Oncogene. 2002; 21(33):5097–5107. [PubMed: 12140760]

Xu X, Weaver Z, Linke SP, Li C, Gotay J, Wang XW, Harris CC, Ried T, Deng CX. Centrosome amplification and a defective G2-M cell cycle checkpoint induce genetic instability in BRCA1 exon 11 isoform-deficient cells. Mol Cell. 1999; 3(3):389–395. [PubMed: 10198641]

Zhou H, Kuang J, Zhong L, Kuo W-L, Gray JW, Sahin A, Brinkely BR, Sen S. Tumor amplified kinase STK15/BTAK induces centrosome amplification, aneuploidy and transformation. Nature Genetics. 1998; 20:189–193. [PubMed: 9771714]

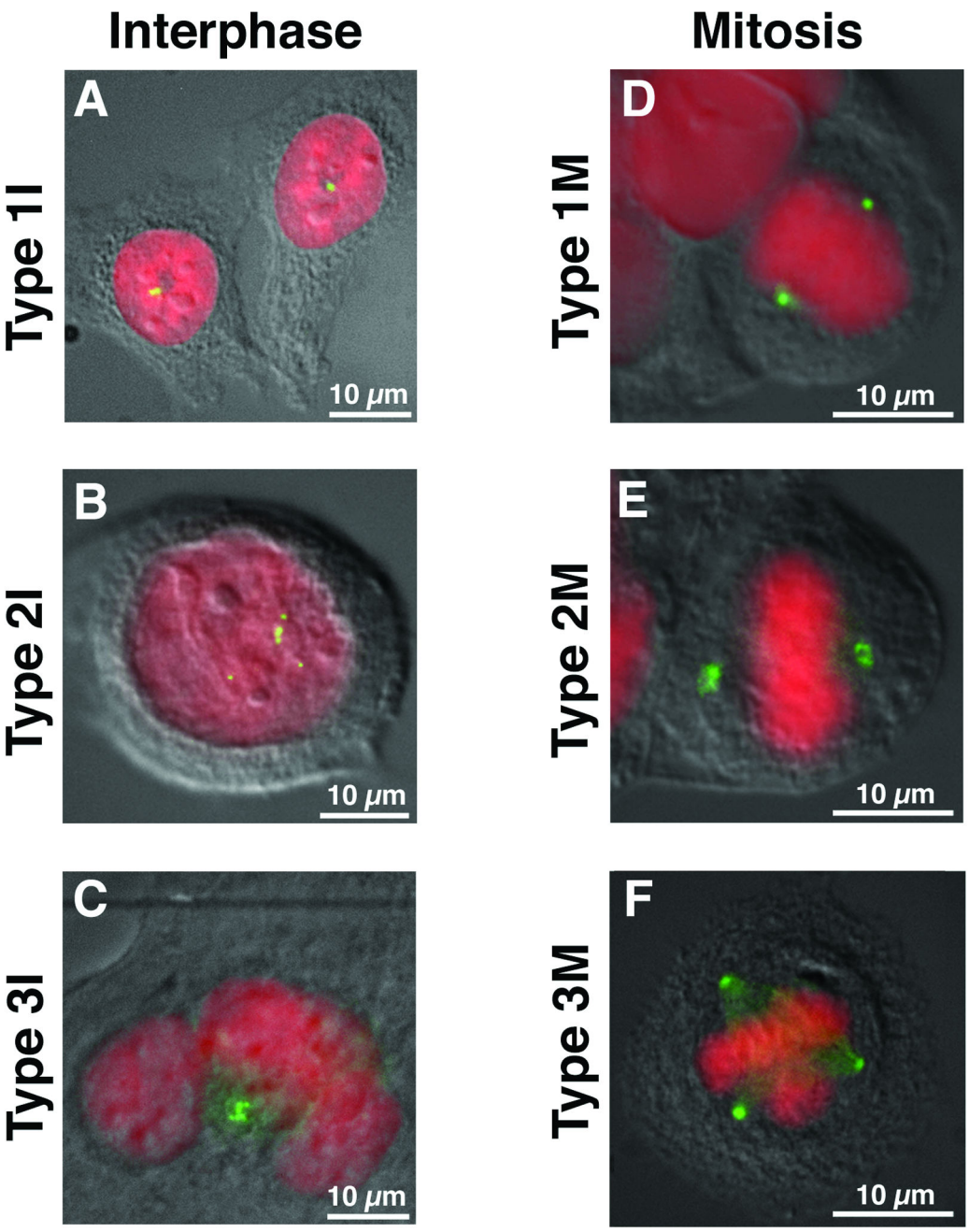

Figure 1.

Interphase cells (I) were categorized based on the number of their centrosomes (green) as detected with an anti-γ-tubulin antibody. DNA was counterstained with DAPI (red) and the cells visualized by differential interference contrast (DIC) microscopy. Type 1I (A) have 1–2 centrosomes. Type 2I (B) are mono-nucleated cells with multiple centrosomes while Type 3I (C) contain multiple centrosomes in a multi-nucleated cell. Mitotic cells (M) were categorized in a similar manner based on the number and orientation of their centrosomes with respect to the mitotic plate. Type 1M (D) have a bi-polar spindle with 1 centrosome on

either side of the mitotic plate. Type 2M (E) mitoses are bi-polar but demonstrate coalescence of multiple centrosomes at either pole. Type 3M (F) are multipolar mitoses in which the chromosomes are pulled in more than two directions.

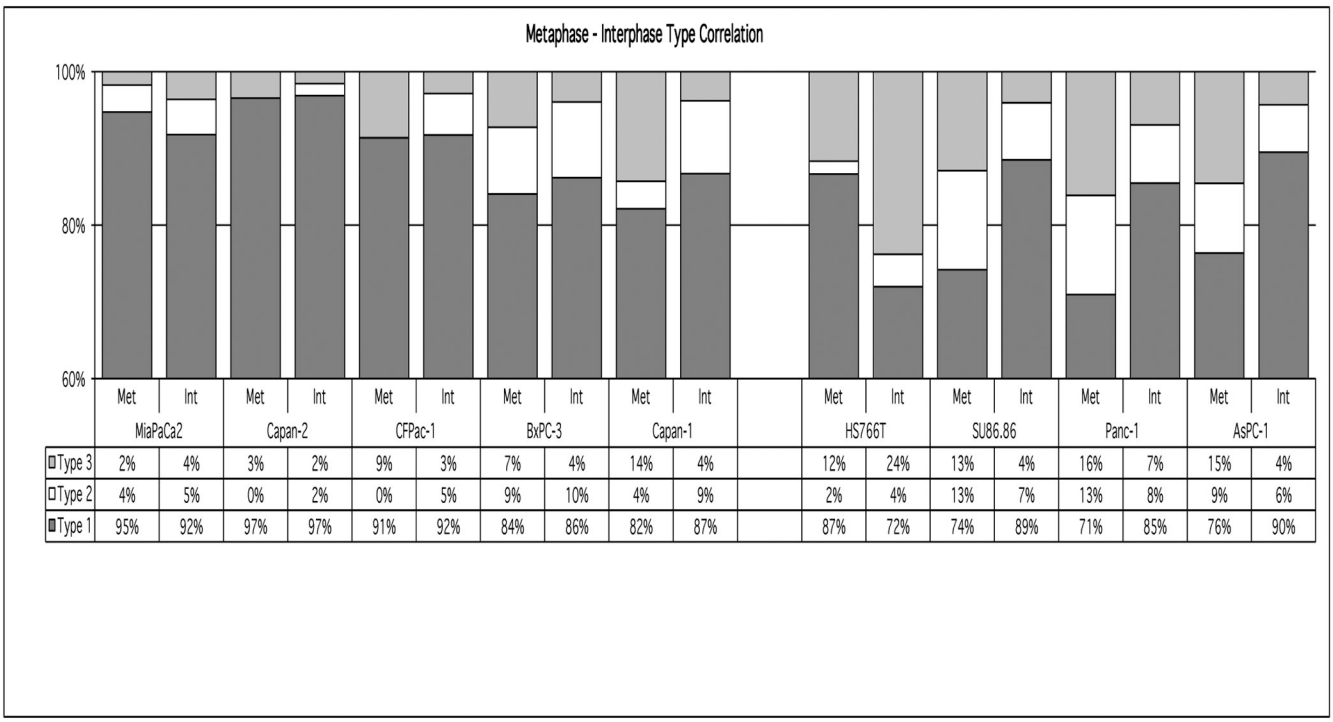

	Met	Int	Met	Int	Met	Int	Met	Int	Met	Int		Met	Int	Met	Int	Met	Int	Met	Int
	MiaPaCa2		Capan-2		CFPac-1		BxPC-3		Capan-1			HS766T		SU86.86		Panc-1		AsPC-1	
Type 3	2%	4%	3%	2%	9%	3%	7%	4%	14%	4%		12%	24%	13%	4%	16%	7%	15%	4%
Type 2	4%	5%	0%	2%	0%	5%	9%	10%	4%	9%		2%	4%	13%	7%	13%	8%	9%	6%
Type 1	95%	92%	97%	97%	91%	92%	84%	86%	82%	87%		87%	72%	74%	89%	71%	85%	76%	90%

Figure 2.

Quantitation and comparison of interphase (Int) (n≥300) and metaphase (Met) (n≥50) pancreatic cancer cells based on the categories illustrated in Figure 1.

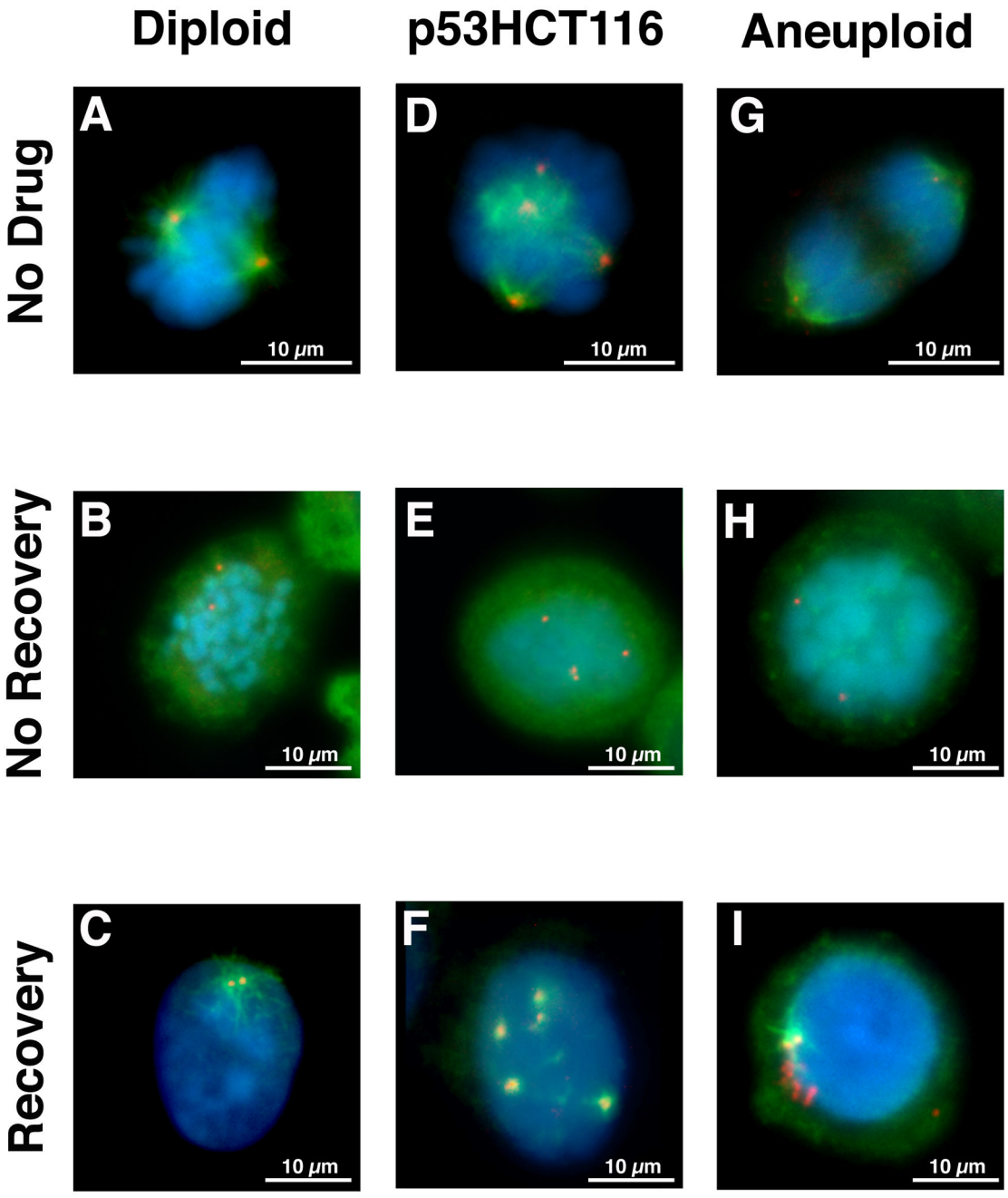

Figure 3.

Nucleation assay and subsequent detection of both α-tubulin spindles (green) and γ-tubulin (red) in diploid (A–C) and aneuploid (G–I) colorectal cancer cell lines as well as p53HCT116 (D–F), a diploid colorectal cell line made homozygous deficient for *TP53*. Untreated cells (A, D, G) in mitosis reveal mitotic spindles nucleating from the centrosomes. Nocodazole treated cells (B, E, H) in mitosis. The absence of mitotic spindles demonstrates the microtubule depolymerizing activity of the drug. Cells allowed to briefly recover from nocodazole treatment (C, F, I) reveal nucleation of α-tubulin containing microtubules from

all γ-tubulin structures in the diploid (C) and p53HCT116 (F) cells compared to only 1–2 γ-tubulin structures in the aneuploid colorectal cell lines (I).

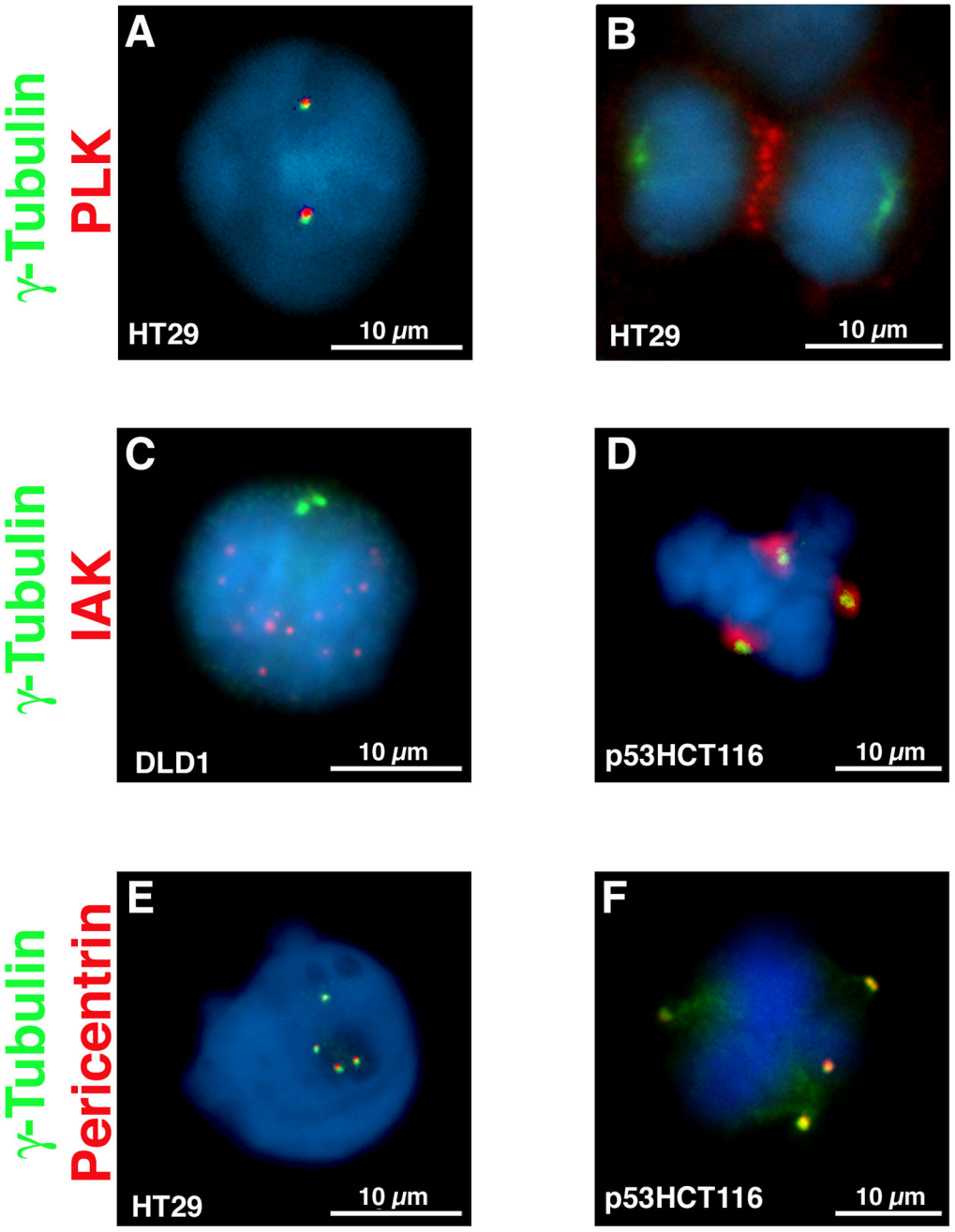

Figure 4.

Dual immunofluorescence for γ-tubulin and Polo-like kinase 1 (PLK1) (A &B), Aurora-kinase A (AURKA) (C & D) and PCNT (E & F). Interphase cells reveal co-localization of γ-tubulin with PLK1 (A) and PCNT (E) but not with AURKA (C). In mitosis, however, all four protein co-localize (D & E), however PLK1 remains at the metaphase plate during anaphase (B) and is found as two rings at the midbody after cytokinesis.

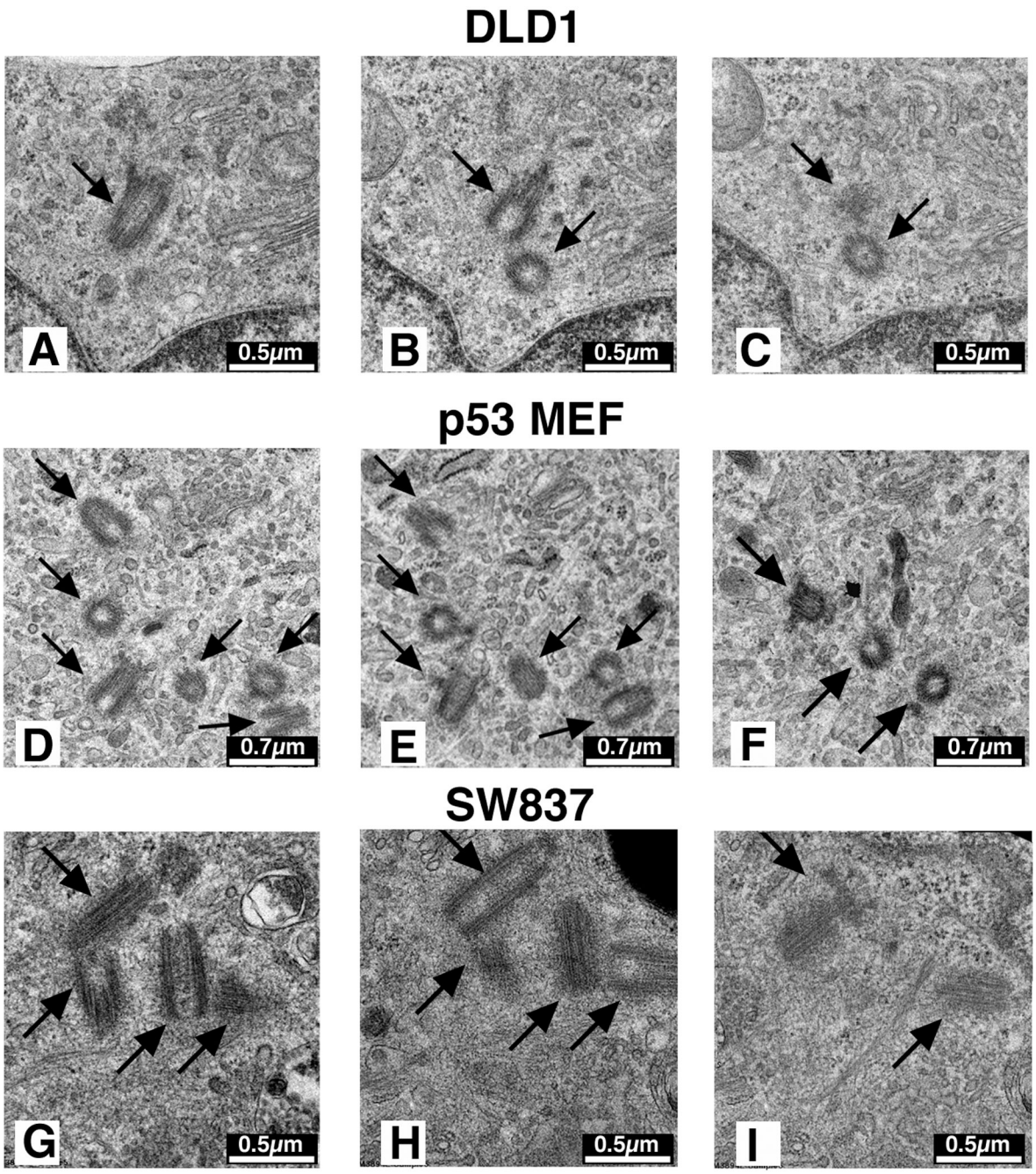

Figure 5.

Electron microscopic serial sections of centrioles. One centriole pair, in their normal perpendicular orientation, as illustrated in the diploid cell line DLD1 (A – C). In *Trp53*-deficient MEFs (D – F) and the *TP53*-deficient HCT116 cell line (data not shown), multiple pairs of centrioles were observed, sometimes in clusters. Three pairs of centrosomes are depicted here. In the aneuploid colorectal cancer cell lines, such as shown for SW837 (G – I), two pairs of centrosomes were also observed, even in cells with multiple γ-tubulin foci.

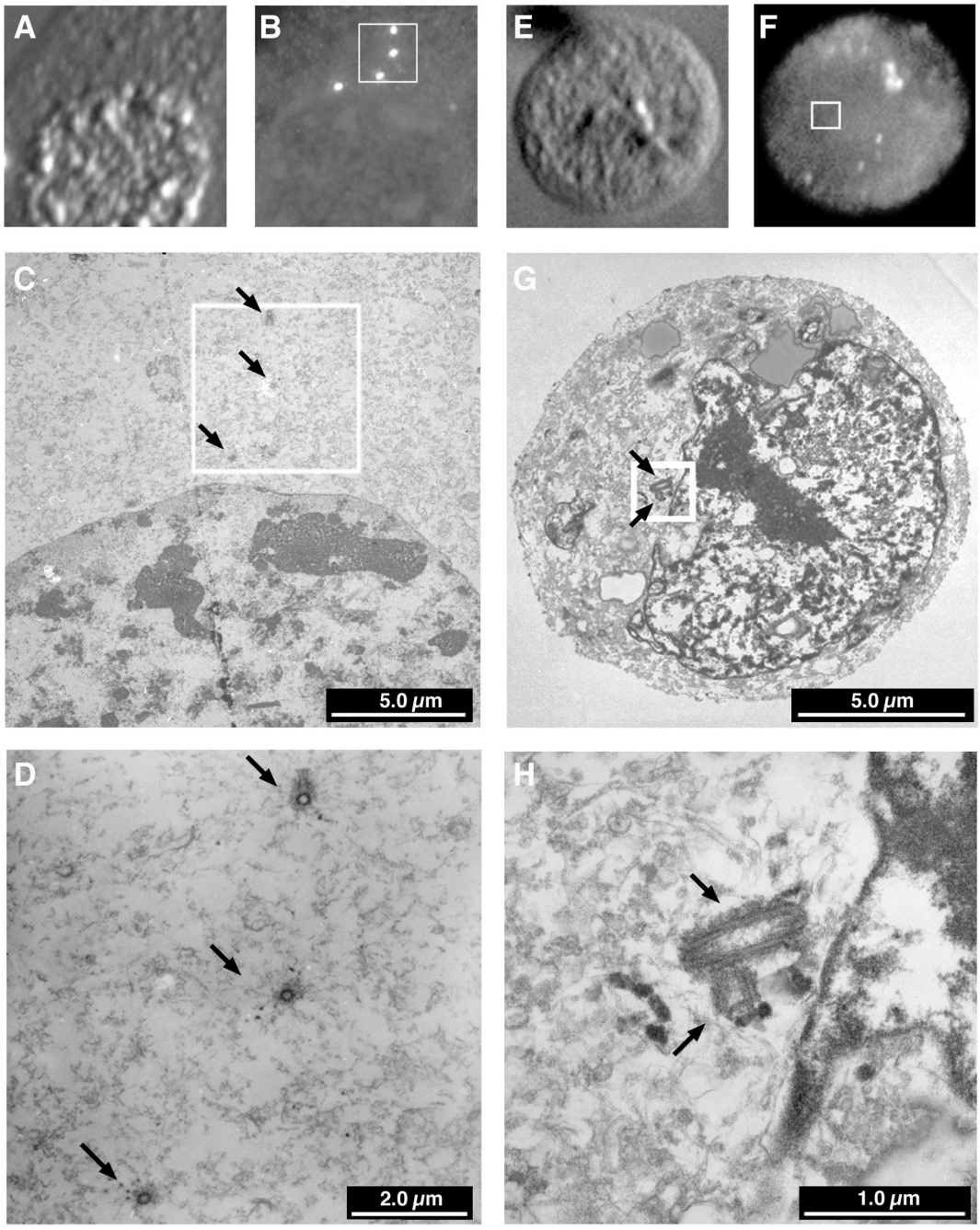

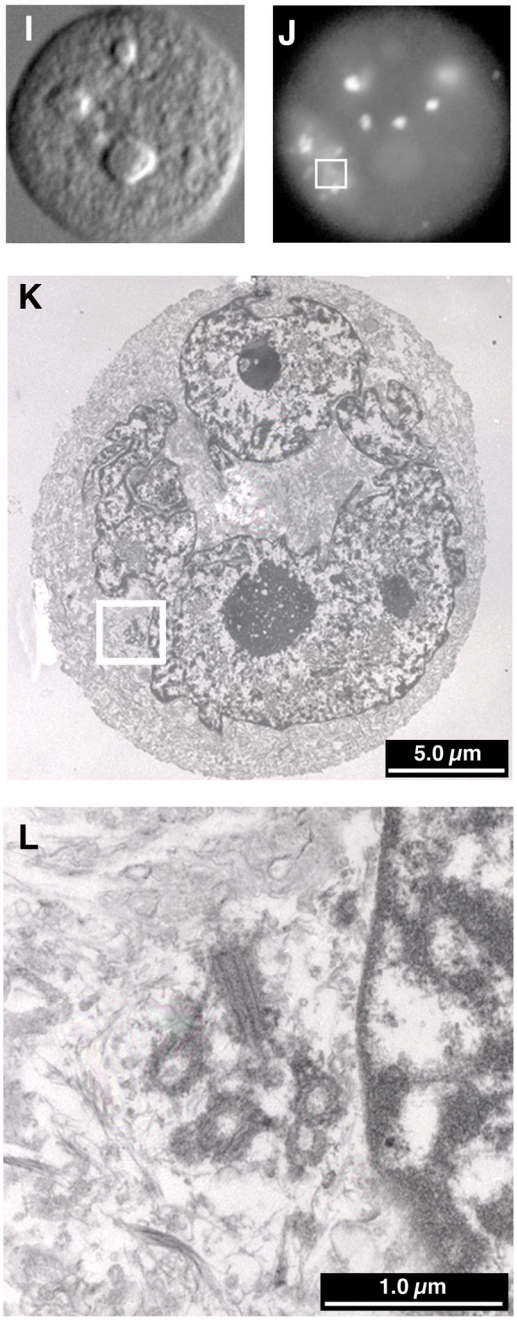

Figure 6.

Immunocytochemistry - Electron microscopy (ICC-EM)

Differential interference contrast (DIC) (A, E & I) and immunofluorescence detection of γ-tubulin (B, F & J) was followed by preparation of serial sections for EM and relocalization of the cells with the aid of gridded coverslips. In *Trp53*-deficient MEFs (A-D) and the cell line p53HCT116 (data not shown), every pair of centrioles corresponded to a γ-tubulin structure. Aneuploid colorectal cells containing multiple γ-tubulin structures usually contained one or two correctly oriented centriole pairs (E-H). Very rarely, however, a cell

was observed which contained a cluster of centrioles (I-L), but in association with only one of the many γ-tubulin structures, the others being devoid of centrioles.

Table I

Comparison of centrosome aberrations during mitosis and interphase in pancreatic cell lines.

	Interphase Nuclei	Mitoses
Cell Line	**Observed Abnormal[a]**	**Observed Multipolar[b]**
AsPC-1	10%	15%
BxPC-3	14%	7%
Capan-1	13%	9%
Capan-2	3%	3%
CFPac-1	8%	9%
Hs766T	28%	19%
Mia PaCa-2	8%	2%
Panc-1	15%	16%
SU86.86	11%	13%

[a] Type2 and Type3 interphase cells combined.

[b] Type3 metaphase cells.

Environ Mol Mutagen. Author manuscript; available in PMC 2015 February 10.

Table 2

Gene Name	Map Position	DvM Linear Ratio	DvM P- value	AvM Linear Ratio	AvM P value	AvD Linear Ratio	AvD P value	TvM Linear Ratio	TvM P value	Description
ACTR1A	chr10:104229479-104229420	0.539647305	0.018696017	0.550153772	0.0010171	1.019469136	0.929200173	0.549205278	0.008497794	Homo sapiens ARP1 actin-related protein 1 homolog A, centractin alpha (yeast) (ACTR1A), mRNA [NM_005736]
ACTR1A	chr10:104230605-104230546	1.04608995	0.818342947	0.648466369	0.008279034	0.61989542	0.042939928	0.699012881	0.00666194	Homo sapiens ARP1 actin-related protein 1 homolog A, centractin alpha (yeast) (ACTR1A), mRNA [NM_005736]
ACTR1A	chr10:104235454-104235395	1.22501463	0.414176537	0.895646251	0.558158895	0.731131065	0.191056088	0.583951097	0.024949017	Homo sapiens ARP1 actin-related protein 1 homolog A, centractin alpha (yeast) (ACTR1A), mRNA [NM_005736]
ACTR1B	chr2:97731657-97731598	0.659558652	0.038408023	0.843711821	0.311689899	1.279206661	0.173222468	0.783190459	0.350625827	Homo sapiens ARP1 actin-related protein 1 homolog B, centractin beta (yeast) (ACTR1B), mRNA [NM_005735]
ASPM	chr1:193785170-193785111	10.77544985	***4.44757E-06***	7.890656212	0.000300598	0.732280909	0.459948772	8.31922161	***3.8004E-06***	Homo sapiens asp (abnormal spindle)-like, microcephaly associated (Drosophila) (ASPM), mRNA [NM_018136]
ASPM	chr1:193844840-193844781	4.633452771	***1.78125E-05***	2.596709011	0.019904575	0.560426347	0.131647348	5.120339502	0.000480597	Homo sapiens asp (abnormal spindle)-like, microcephaly associated (Drosophila) (ASPM), mRNA [NM_018136]
AURKA	chr20:54378586-54378527	5.033885486	0.000217951	5.096766692	***2.44615E-05***	1.012491585	0.963262042	8.378408936	***1.93798E-09***	Homo sapiens aurora kinase A (AURKA), transcript variant 1,

Gene Name	Map Position	DvM Linear Ratio	DvM P- value	AvM Linear Ratio	AvM P value	AvD Linear Ratio	AvD P value	TvM Linear Ratio	TvM P value	Description
										mRNA [NM_198433] mRNA [NM_198433]
AURKAIP1	chr1:1349349-1349193	0.875588444	0.432692593	0.892538657	0.491899499	1.019358654	0.889299865	1.344257482	0.19504244	Homo sapiens aurora kinase A interacting protein 1 (AURKAIP1), mRNA [NM_017900]
AURKB	chr17:8051642-8051380	7.872273192	0.000490426	5.595317117	0.000234224	0.710762569	0.399696704	5.433402537	***4.42256E-05***	Homo sapiens aurora kinase B (AURKB), mRNA [NM_004217]
AURKC	chr19:62435754-62435813	1.21624842	0.57975991	0.912809485	0.542426431	0.75051237	0.449794723	0.19721149	0.08925087	Homo sapiens aurora kinase C (AURKC), transcript variant 1, mRNA [NM_001015878]
CCDC5	chr18:41957282-41958798	2.693528404	0.001496512	2.034856415	0.018498786	0.75546128	0.264585612	0.978815227	0.897631526	Homo sapiens coiled-coil domain containing 5 (spindle associated) (CCDC5), mRNA [NM_138443]
CEND1	chr11:778062-778003	0.507068172	0.308536962	0.610988619	0.315812795	1.20494374	0.780149802	0.027157738	***2.05961E-11***	Homo sapiens cell cycle exit and neuronal differentiation 1 (CEND1), mRNA [NM_016564]
CEND1	chr11:778360-778301	0.968945488	0.660559255	1.278257171	0.104024766	1.319225062	0.086664261	1.425476559	0.006553738	Homo sapiens cell cycle exit and neuronal differentiation 1 (CEND1), mRNA [NM_016564]
CENPA	chr2:26928565-26928624	14.66658432	***2.16592E-05***	11.34106026	***8.24114E-05***	0.77325845	0.526011482	9.892367239	***1.58309E-06***	Homo sapiens centromere protein A (CENPA), transcript variant 1, mRNA [NM_001809]
CENPB	chr20:3713453-3713394	0.760030198	0.159655839	1.180472313	0.266016213	1.553191328	0.046935865	0.5537266	0.013168675	Homo sapiens centromere protein B, 80kDa (CENPB), mRNA [NM_001810]

Gene Name	Map Position	DvM Linear Ratio	DvM P- value	AvM Linear Ratio	AvM P value	AvD Linear Ratio	AvD P value	TvM Linear Ratio	TvM P value	Description
CENPB	chr20:3715043-3714984	1.160296316	0.363689859	1.185731237	0.340074488	1.021921057	0.845679736	0.73662732	0.001802347	Homo sapiens centromere protein B, 80kDa (CENPB), mRNA [NM_001810]
CENPC1	chr4:68169448-68169389	1.160612838	0.405485687	1.059114704	0.684977297	0.912547811	0.624082623	1.118880269	0.372545452	Homo sapiens centromere protein C 1 (CENPC1), mRNA [NM_001812]
CENPC1	chr4:68188382-68187437	1.006709055	0.934194201	0.876358785	0.358993464	0.870518429	0.332645481	0.851713879	0.289385268	Homo sapiens centromere protein C 1 (CENPC1), mRNA [NM_001812]
CENPE	chr4:104385002-104384943	5.080925974	***3.94403E-06***	3.963894178	0.001133087	0.780151925	0.449791506	5.788419262	***4.83071E-07***	Homo sapiens centromere protein E, 312kDa (CENPE), mRNA [NM_001813]
CENPF	chr1:211214634-211214693	13.31623126	***6.81039E-06***	8.593518485	***1.4088E-05***	0.645341638	0.139738593	9.487805522	0.000145524	Homo sapiens centromere protein F, 350/400ka (mitosin) (CENPF), mRNA [NM_016343]
CENPF	chr1:211225703-211225762	15.29546784	***1.87815E-07***	8.370579827	0.00026139	0.547258829	0.147519816	10.40332935	***1.61432E-06***	Homo sapiens centromere protein F, 350/400ka (mitosin) (CENPF), mRNA [NM_016343]
CENPH	chr5:68541405-68541464	9.107266658	0.000127541	7.245875049	***9.04981E-05***	0.79561468	0.503731509	6.864131023	0.001168224	Homo sapiens centromere protein H (CENPH), mRNA [NM_022909]
CENPI	chrX:100193585-100201853	4.931762582	0.009120648	6.641217038	***1.89721E-05***	1.346621401	0.492460004	15.96776733	0.022712509	Homo sapiens centromere protein I (CENPI), mRNA [NM_006733]
CENPI	chrX:100222701-100224023	5.244225042	0.002512297	5.004508063	0.002597057	0.954289342	0.893063222	12.55296847	0.042236629	Homo sapiens centromere protein I (CENPI), mRNA [NM_006733]
CENPJ	chr13:24355465-24355406	1.922398211	0.015693791	2.160038313	0.02897501	1.123616481	0.722112884	3.433376648	0.001048035	Homo sapiens centromere protein

Gene Name	Map Position	DvM Linear Ratio	DvM P- value	AvM Linear Ratio	AvM P value	AvD Linear Ratio	AvD P value	TvM Linear Ratio	TvM P value	Description
										J (CENPJ), mRNA [NM_018451]
CENPJ	chr13:24361516-24361457	2.375437864	0.009754441	2.66206312	0.008230167	1.120662073	0.659930266	2.450784398	0.043428847	Homo sapiens centromere protein J (CENPJ), mRNA [NM_018451]
CENPK	chr5:64849628-64849569	13.37245646	0.028684671	14.21561885	0.017558405	1.063052169	0.871131403	24.60140419	0.02444757	Homo sapiens centromere protein K (CENPK), mRNA [NM_022145]
CENPL	chr1:170503839-170503780	8.302882521	***3.66873E-05***	7.378983166	***3.66157E-05***	0.888725469	0.704008813	10.18527728	0.026056405	Homo sapiens centromere protein L (CENPL), mRNA [NM_033319]
CENPM	chr22:40666456-40665789	5.553492008	***2.62399E-07***	3.998953137	0.000247492	0.72007903	0.223876047	8.952540978	***6.72703E-06***	Homo sapiens centromere protein M (CENPM), transcript variant 2, mRNA [NM_001002876]
CENPN	chr16:79598381-79603092	8.210107056	***1.78164E-05***	6.192759908	***5.47473E-05***	0.754284916	0.361160034	5.703264764	***1.02245E-09***	Homo sapiens centromere protein N (CENPN), mRNA [NM_018455]
CENPN	chr16:79611372-79613909	5.821282605	***3.28212E-05***	4.440301964	0.000330328	0.762770383	0.379305925	6.851514614	***4.41852E-12***	Homo sapiens centromere protein N (CENPN), mRNA [NM_018455]
CENPO	chr2:24952223-24952282	9.686741435	***3.2314E-08***	5.299169032	***8.30294E-06***	0.547053833	0.017438259	6.06202778	***1.69889E-07***	Homo sapiens centromere protein O (CENPO), mRNA [NM_024322]
CENPP	chr9:92455060-92455119	2.88776894	0.000365082	2.467694847	0.005898249	0.854533343	0.581288593	3.776965241	***3.8881E-05***	Homo sapiens centromere protein P (CENPP), mRNA [NM_001012267]
CENPQ	chr6:49564899-49564958	2.889926614	0.023577043	2.512399172	0.037472542	0.86936435	0.474572539	1.725225203	0.154183717	Homo sapiens centromere protein Q (CENPQ), mRNA [NM_018132]

Gene Name	Map Position	DvM Linear Ratio	DvM P- value	AvM Linear Ratio	AvM P value	AvD Linear Ratio	AvD P value	TvM Linear Ratio	TvM P value	Description
CENPT	chr16:66420143-66420084	1.022674924	0.788129804	1.175371187	0.304488725	1.149310655	0.321525946	1.824092922	0.017936524	Homo sapiens centromere protein T (CENPT), mRNA [NM_025082]
CENPT	chr16:66421431-66421372	0.473186734	0.002043084	0.434525475	0.000711106	0.918295979	0.587202789	1.368268765	0.259911193	Homo sapiens centromere protein T (CENPT), mRNA [NM_025082]
CENTA1	chr7:711648-711589	1.861216881	0.100760409	2.566091142	0.022704163	1.378716885	0.239573316	2.914059777	0.021788012	Homo sapiens centaurin, alpha 1 (CENTA1), mRNA [NM_006869]
CENTA2	chr17:26309305-26309364	0.149897375	0.024326925	0.061964964	***2.16546E-06***	0.413382579	0.202638744	0.587337492	0.006963379	Homo sapiens centaurin, alpha 2 (CENTA2), mRNA [NM_018404]
CENTA2	chr17:26310276-26310335	0.4199129	0.249417153	0.066723052	***6.24645E-06***	0.158897361	0.039242308	0.58464795	0.065301568	Homo sapiens centaurin, alpha 2 (CENTA2), mRNA [NM_018404]
CENTB1	chr17:7191975-7192034	0.171301006	0.071517643	0.26397975	0.005963217	1.541028597	0.52189905	0.179123258	0.000434957	Homo sapiens centaurin, beta 1 (CENTB1), mRNA [NM_014716]
CENTB2	chr3:196477804-196477745	1.215686466	0.25098198	1.133828417	0.44386769	0.932665164	0.73061917	0.9186657	0.603597594	Homo sapiens centaurin, beta 2 (CENTB2), mRNA [NM_012287]
CENTB2	chr3:196480818-196480759	1.722939411	0.072313546	1.321469794	0.299997347	0.766985644	0.204891151	1.505341683	0.025996821	Homo sapiens centaurin, beta 2 (CENTB2), mRNA [NM_012287]
CENTB5	chr1:1269141-1268968	0.742843194	0.148353944	1.166081003	0.54117673	1.569753903	0.10821532	1.182467327	0.511673526	Homo sapiens centaurin, beta 5 (CENTB5), mRNA [NM_030649]
CENTB5	chr1:1269725-1269464	0.810471647	0.101784782	1.281318849	0.191679191	1.580954564	0.02038519	1.29718021	0.145506597	Homo sapiens centaurin, beta 5 (CENTB5), mRNA [NM_030649]
CENTB5	chr1:1275204-1275145	0.74540625	0.518379615	1.265706798	0.209817071	1.698009372	0.276853635	0.624373851	0.045615315	Homo sapiens centaurin, beta 5 (CENTB5), mRNA [NM_030649]

Gene Name	Map Position	DvM Linear Ratio	DvM P- value	AvM Linear Ratio	AvM P value	AvD Linear Ratio	AvD P value	TvM Linear Ratio	TvM P value	Description
CENTB5	chr1:1277325-1275971	0.571072233	0.103770254	1.016373128	0.959436592	1.779762819	0.103733989	1.529327654	0.298978196	Homo sapiens centaurin, beta 5 (CENTB5), mRNA [NM_030649]
CENTD1	chr4:35890726-35890667	1.189865863	0.631663062	0.914683837	0.843478164	0.768728531	0.548536713	1.089223467	0.730138206	Homo sapiens centaurin, delta 1 (CENTD1), transcript variant 1, mRNA [NM_015230]
CENTD2	chr11:72073969-72073910	0.614070574	0.005408387	0.78701812	0.138614721	1.281641155	0.06546912	1.089927256	0.665474482	Homo sapiens centaurin, delta 2 (CENTD2), transcript variant 1, mRNA [NM_139181]
CENTD2	chr11:72074816-72074757	0.682167982	0.068049339	0.849583364	0.278080925	1.245416651	0.233612347	1.029541083	0.905644527	Homo sapiens centaurin, delta 2 (CENTD2), transcript variant 1, mRNA [NM_139181]
CENTD3	chr5:141013392-141013333	0.846143717	0.687687124	0.256973382	0.011218199	0.303699451	0.030830875	1.622820712	0.123428198	Homo sapiens centaurin, delta 3 (CENTD3), mRNA [NM_022481]
CENTG2	chr2:236815264-236815323	1.120771695	0.577704518	1.536917553	0.060203036	1.37130297	0.097805525	0.906022093	0.716329509	Homo sapiens centaurin, gamma 2 (CENTG2), transcript variant 2, mRNA [NM_014914]
CENTG2	chr2:236815985-236816043	0.878484028	0.448048591	1.023844397	0.897372888	1.165467287	0.221551269	1.214583463	0.39520102	Homo sapiens centaurin, gamma 2 (CENTG2), transcript variant 1, mRNA [NM_001037131]
CENTG3	chr7:150258174-150258233	0.647034429	0.019168303	0.56762896	0.003069559	0.877277829	0.311762193	0.628322942	0.116838387	Homo sapiens centaurin, gamma 3 (CENTG3), transcript variant 2, mRNA [NM_001042535]
CENTG3	chr7:150277356-150278121	1.247523599	0.330094239	1.686018723	0.050028366	1.351492449	0.253837315	1.170336749	0.506022938	Homo sapiens centaurin, gamma 3 (CENTG3), transcript variant 1,

Gene Name	Map Position	DvM Linear Ratio	DvM P- value	AvM Linear Ratio	AvM P value	AvD Linear Ratio	AvD P value	TvM Linear Ratio	TvM P value	Description
										mRNA [NM_031946] mRNA [NM_031946]
CENTG3	chr7:150279082-150279141	1.330930748	0.225453403	1.606891551	0.024721051	1.207344224	0.436969359	1.75815973	0.024665984	Homo sapiens centaurin, gamma 3 (CENTG3), transcript variant 1, mRNA [NM_031946]
CEP110	chr9:120938376-120940257	1.903514736	0.030865732	1.093647861	0.746872002	0.574541316	0.087998296	1.285331062	0.235830586	Homo sapiens centrosomal protein 110kDa (CEP110), mRNA [NM_007018]
CEP110	chr9:121015240-121015299	2.125447106	0.002437274	2.277011447	0.005969369	1.071309392	0.792661283	1.399054603	0.201796018	Homo sapiens centrosomal protein 110kDa (CEP110), mRNA [NM_007018]
CEP135	chr4:56740039-56740098	1.99879018	0.007840708	1.465343529	0.083959271	0.733115233	0.174405033	1.272069603	0.486322049	Homo sapiens centrosomal protein 135kDa (CEP135), mRNA [NM_025009]
CEP152	chr15:46818050-46817991	6.365304608	0.001010772	3.701976961	0.000342989	0.581586772	0.158150536	4.651734824	0.000154524	Homo sapiens centrosomal protein 152kDa (CEP152), mRNA [NM_014985]
CEP152	chr15:46835606-46835547	2.86387685	0.001660254	1.441871446	0.085179057	0.503468383	0.01677613	3.16611472	0.000112429	Homo sapiens centrosomal protein 152kDa (CEP152), mRNA [NM_014985]
CEP152	chr15:46876919-46876860	5.763911938	0.002469072	3.48895092	0.004439811	0.605309546	0.194190182	9.412200382	0.057854157	Homo sapiens centrosomal protein 152kDa (CEP152), mRNA [NM_014985]
CEP164	chr11:116787812-116788025	1.777902045	0.014046533	1.800247354	***5.80363E-05***	1.012568357	0.943495956	1.475793024	0.020343957	Homo sapiens centrosomal protein 164kDa (CEP164), mRNA [NM_014956]

Gene Name	Map Position	DvM Linear Ratio	DvM P- value	AvM Linear Ratio	AvM P value	AvD Linear Ratio	AvD P value	TvM Linear Ratio	TvM P value	Description
CEP164	chr11:116788900-116788959	1.498076302	0.024992294	1.657991545	0.003670385	1.106747061	0.503469266	2.492997648	0.001292073	Homo sapiens centrosomal protein 164kDa (CEP164), mRNA [NM_014956]
CEP170	chr1:239615116-239615057	1.421950437	0.317851909	1.161020047	0.687824677	0.816498253	0.526860729	0.71943127	0.407049036	Homo sapiens centrosomal protein 170kDa (CEP170), transcript variant alpha, mRNA [NM_014812]
CEP170	chr1:239615751-239615693	1.238051333	0.482605789	1.440667912	0.222881189	1.163657656	0.530740462	0.922267283	0.861385217	Homo sapiens centrosomal protein 170kDa (CEP170), transcript variant alpha, mRNA [NM_014812]
CEP170	chr1:239615909-239615850	2.671694398	0.018583254	2.069706728	0.060888338	0.774679443	0.355862574	1.05375875	0.951032725	Homo sapiens centrosomal protein 170kDa (CEP170), transcript variant alpha, mRNA [NM_014812]
CEP192	chr18:13114695-13114754	2.388743046	0.008390604	1.985524549	0.002282799	0.831200556	0.446086642	1.84448137	0.021286845	Homo sapiens centrosomal protein 192kDa (CEP192), transcript variant 2, mRNA [NM_018069]
CEP250	chr20:33518300-33518590	1.644863155	0.039344698	1.832296492	0.002207924	1.113950718	0.635026044	2.367640393	0.00048323	Homo sapiens centrosomal protein 250kDa (CEP250), transcript variant 1, mRNA [NM_007186]
CEP250	chr20:33562995-33563054	1.388370642	0.051002882	1.424900352	0.058394494	1.026311209	0.881085598	3.035913597	0.000564547	Homo sapiens centrosomal protein 250kDa (CEP250), transcript variant 1, mRNA [NM_007186]
CEP27	chr15:40640846-40643251	4.880353597	***6.12646E-06***	3.564077959	***3.7139E-06***	0.730290928	0.021523266	2.216863674	***3.22586E-06***	Homo sapiens centrosomal protein 27kDa (CEP27), mRNA [NM_018097]
CEP290	chr12:86945362-86945303	2.482050252	0.001844159	1.719359227	0.005551278	0.692717331	0.077176961	1.560414439	0.022656252	Homo sapiens centrosomal protein

Gene Name	Map Position	DvM Linear Ratio	DvM P- value	AvM Linear Ratio	AvM P value	AvD Linear Ratio	AvD P value	TvM Linear Ratio	TvM P value	Description
										290kDa (CEP290), mRNA [NM_025114]
										290kDa (CEP290), mRNA [NM_025114]
										290kDa (CEP290), mRNA [NM_025114]
CEP290	chr12:86990086-86990027	2.13299736	0.046439019	1.240500022	0.228630892	0.581575976	0.114019801	1.161237974	0.40539539	Homo sapiens centrosomal protein 290kDa (CEP290), mRNA [NM_025114]
CEP290	chr12:87007554-87007495	1.775771373	0.014549972	1.146451569	0.305207578	0.645607642	0.03979151	1.335703384	0.15972627	Homo sapiens centrosomal protein 290kDa (CEP290), mRNA [NM_025114]
CEP350	chr1:176813814-176813873	0.602432222	0.031185402	0.750128266	0.121492348	1.245166242	0.180520516	0.793239701	0.36640114	Homo sapiens centrosomal protein 350kDa (CEP350), mRNA [NM_014810]
CEP55	chr10:95278744-95278803	15.24264981	***5.10241E-06***	9.267558577	0.000134993	0.608001803	0.250198277	9.489143833	***4.0384E-09***	Homo sapiens centrosomal protein 55kDa (CEP55), mRNA [NM_018131]
CEP57	chr11:95195182-95195241	3.754974244	0.002205218	3.483850989	0.002501611	0.927796241	0.735439741	0.966981407	0.907651468	Homo sapiens centrosomal protein 57kDa, mRNA (cDNA clone MGC:47657 IMAGE:5415088), complete cds. [BC039711]
CEP57	chr11:95204441-95204500	1.336414985	0.151671351	1.526372732	0.002837711	1.142139792	0.483345057	0.963759505	0.794560563	Homo sapiens centrosomal protein 57kDa (CEP57), mRNA [NM_014679]
CEP63	chr3:135708732-135708791	0.760254948	0.250754967	0.687965536	0.020752188	0.90491425	0.657505573	0.917784601	0.510706156	Homo sapiens centrosomal protein 63kDa (CEP63), transcript variant 1, mRNA [NM_025180]
CEP63	chr3:135751687-135751746	0.78571475	0.230862624	0.901251733	0.48501956	1.147046983	0.443665717	0.716637178	0.035471074	Homo sapiens centrosomal protein 63kDa (CEP63), transcript variant 1, mRNA [NM_025180]

Gene Name	Map Position	DvM Linear Ratio	DvM P- value	AvM Linear Ratio	AvM P value	AvD Linear Ratio	AvD P value	TvM Linear Ratio	TvM P value	Description
CEP68	chr2:65211270-65211329	1.428281542	0.009524892	1.155090073	0.468734657	0.808727159	0.281613256	1.297912414	0.389265625	Homo sapiens centrosomal protein 68kDa (CEP68), mRNA [NM_015147]
CEP70	chr3:139702062-139702003	1.324438542	0.184212325	0.849397439	0.488493314	0.641326428	0.100758416	0.63599027	0.012980306	Homo sapiens centrosomal protein 70kDa (CEP70), mRNA [NM_024491]
CEP70	chr3:139771888-139738859	1.430083122	0.254485206	0.963065396	0.869853138	0.67343316	0.234549471	0.635790888	0.025818277	Homo sapiens centrosomal protein 70kDa (CEP70), mRNA [NM_024491]
CEP72	chr5:706323-706382	8.032716663	0.000101596	8.289461078	***1.92135E-07***	1.031962339	0.903396806	10.25139941	***3.41397E-08***	Homo sapiens centrosomal protein 72kDa (CEP72), mRNA [NM_018140]
CEP76	chr18:12664543-12663452	4.339251362	0.00224282	3.798982475	***2.62339E-05***	0.875492604	0.675830323	1.252748527	0.154761209	Homo sapiens centrosomal protein 76kDa (CEP76), mRNA [NM_024899]
CEP78	chr9:78115584-78115643	4.846245748	0.001425178	2.206902652	0.033235032	0.455383975	***0.003817319***	2.382707804	0.013801704	Homo sapiens centrosomal protein 78kDa, mRNA (cDNA clone IMAGE:6194709), complete cds. [BC091515]
CETN1	chr18:571466-571525	n/a	n/a	n/a	n/a	n/a	n/a	1.161456539	n/a	Homo sapiens centrin, EF-hand protein, 1 (CETN1), mRNA [NM_004066]
CETN2	chrX:151666808-151666749	0.501943496	0.008099263	1.119875238	0.58234511	2.231078295	***0.000104316***	1.049006507	0.776719386	Homo sapiens centrin, EF-hand protein, 2 (CETN2), mRNA [NM_004344]
CETN3	chr5:89730993-89730934	3.092503925	0.001160663	1.861321435	0.019098216	0.601881673	0.030064776	1.178904169	0.404238164	Homo sapiens centrin, EF-hand protein, 3 (CDC31 homolog, yeast) (CETN3), mRNA [NM_004365]

Gene Name	Map Position	DvM Linear Ratio	DvM P- value	AvM Linear Ratio	AvM P value	AvD Linear Ratio	AvD P value	TvM Linear Ratio	TvM P value	Description
CKAP1	chr19:41308258-41308461	1.051873377	0.786514087	0.852142898	0.401057334	0.810119276	0.285933167	1.138465716	0.531417602	Homo sapiens cytoskeleton associated protein 1 (CKAP1), mRNA [NM_001281]
CKAP2	chr13:51933864-51933923	11.22581574	***1.46171E-05***	10.48840925	***6.78574E-06***	0.934311545	0.831813717	29.80248539	n/a	Homo sapiens cytoskeleton associated protein 2 (CKAP2), mRNA [NM_018204]
CKAP2	chr13:51948395-51948454	10.54431952	0.000178184	7.947936999	***4.45488E-05***	0.75376481	0.329337053	6.054208437	0.000299478	Homo sapiens cytoskeleton associated protein 2 (CKAP2), mRNA [NM_018204]
CKAP2L	chr2:113212048-113211989	16.97870637	***1.58193E-06***	12.85249895	***3.03004E-05***	0.756977515	0.493586254	12.84382198	***3.24863E-11***	Homo sapiens cytoskeleton associated protein 2-like (CKAP2L), mRNA [NM_152515]
CKAP4	chr12:105134998-105134939	1.192424072	0.539105116	1.693828458	0.128720564	1.420491667	0.399268907	1.465653433	0.067533936	Homo sapiens cytoskeleton-associated protein 4 (CKAP4), mRNA [NM_006825]
CKAP5	chr11:46722100-46722041	2.263895189	***1.42451E-05***	2.165037942	***3.07016E-06***	0.956333116	0.678260735	2.619556866	***3.08061E-05***	Homo sapiens cytoskeleton associated protein 5 (CKAP5), transcript variant 1, mRNA [NM_001008938]
CKAP5	chr11:46728512-46728453	3.593201945	0.000428454	3.563956667	***1.31413E-07***	0.991860942	0.962482903	2.415876152	0.007136492	Homo sapiens cytoskeleton associated protein 5 (CKAP5), transcript variant 1, mRNA [NM_001008938]

Gene Name	Map Position	DvM Linear Ratio	DvM P- value	AvM Linear Ratio	AvM P value	AvD Linear Ratio	AvD P value	TvM Linear Ratio	TvM P value	Description
CNTROB	chr17:7791983-7792219	1.380090445	0.147794125	1.188513785	0.194224222	0.861185431	0.484869864	1.074462385	0.599837685	Homo sapiens centrobin, centrosomal BRCA2 interacting protein (CNTROB), transcript variant 1, mRNA [NM_053051]
CNTROB	chr17:7793143-7793429	1.333007534	0.017272461	1.060273067	0.710207071	0.795399156	0.159160311	1.444629856	0.013689337	Homo sapiens centrobin, centrosomal BRCA2 interacting protein (CNTROB), transcript variant 1, mRNA [NM_053051]
CSPP1	chr8:68170424-68170483	1.85414209	***9.72806E-05***	1.250798595	0.041178529	0.674596948	***0.000490814***	1.822661654	***3.73583E-06***	Homo sapiens centrosome and spindle pole associated protein 1 (CSPP1), mRNA [NM_024790]
CSPP1	chr8:68206803-68206862	1.355004111	0.054170198	0.688085399	0.001863954	0.507810562	***0.001200116***	1.779930558	0.006905074	Homo sapiens centrosome and spindle pole associated protein 1 (CSPP1), mRNA [NM_024790]
CSPP1	chr8:68270186-68270245	2.714129926	0.00047888	1.768188301	0.008985281	0.651475187	***0.009680708***	2.553363272	0.000371821	Homo sapiens centrosome and spindle pole associated protein 1 (CSPP1), mRNA [NM_024790]
CTGLF1	chr10:45641249-45641190	1.714236368	0.125294337	1.107443101	0.7421465	0.646027072	0.171997553	1.113648586	0.731150986	Homo sapiens centaurin, gamma-like family, member 1 (CTGLF1), mRNA [NM_133446]
CTGLF1	chr10:45641325-45641266	1.35765382	0.237411476	1.11543456	0.594186436	0.821589822	0.327373296	1.558620468	0.156626762	Homo sapiens centaurin, gamma-like family, member 1 (CTGLF1), mRNA [NM_133446]

Gene Name	Map Position	DvM Linear Ratio	DvM P- value	AvM Linear Ratio	AvM P value	AvD Linear Ratio	AvD P value	TvM Linear Ratio	TvM P value	Description
CTGLF1	chr10:45641778-45641719	1.251008149	0.1621321	1.021552801	0.87309074	0.81658365	0.123885274	1.468856065	0.113735649	Homo sapiens centaurin, gamma-like family, member 1 (CTGLF1), mRNA [NM_133446]
CTGLF1	chr10:45641831-45641772	1.141674539	0.44921962	0.922871213	0.631865769	0.808348773	0.137003791	1.574802573	0.132495227	Homo sapiens centaurin, gamma-like family, member 1 (CTGLF1), mRNA [NM_133446]
CTGLF1	chr10:45642218-45642159	1.190017741	0.345224548	1.156570148	0.381464493	0.971893198	0.8543206	1.498683585	0.284859853	Homo sapiens centaurin, gamma-like family, member 1 (CTGLF1), mRNA [NM_133446]
CTGLF1	chr10:45642232-45642173	1.174780573	0.312526032	1.2182892	0.204869199	1.037035535	0.761944006	1.360121165	0.324195659	Homo sapiens centaurin, gamma-like family, member 1 (CTGLF1), mRNA [NM_133446]
CTGLF1	chr10:45662203-45662144	1.217208374	0.444876035	1.268216579	0.353921386	1.041905894	0.795047887	2.354166807	0.047087627	Homo sapiens centaurin, gamma-like family, member 1 (CTGLF1), mRNA [NM_133446]
ESPL1	chr12:51950737-51950796	n/a	n/a	n/a	n/a	0.841553567	0.842833898	1.852540929	n/a	Homo sapiens extra spindle poles like 1 (S. cerevisiae) (ESPL1), mRNA [NM_012291]
ESPL1	chr12:51973015-51973376	3.254837903	0.041239758	1.932918036	0.20586329	0.59386	0.075112613	4.05140709	0.082693087	Homo sapiens extra spindle poles like 1 (S. cerevisiae) (ESPL1), mRNA [NM_012291]
GCET2	chr3:113328551-113325307	2.389227262	0.294056971	0.551039068	0.307032374	0.230634849	0.133085603	0.161110006	n/a	Homo sapiens germinal center expressed transcript 2 (GCET2), transcript variant 2, mRNA [NM_001008756]

Gene Name	Map Position	DvM Linear Ratio	DvM P- value	AvM Linear Ratio	AvM P value	AvD Linear Ratio	AvD P value	TvM Linear Ratio	TvM P value	Description
INCENP	chr11:61676318-61676377	3.697943337	***1.33517E-05***	2.832056481	0.000569571	0.76584637	0.235018719	4.941445961	***3.98785E-10***	Homo sapiens inner centromere protein antigens 135/155kDa (INCENP), transcript variant 2, mRNA [NM_020238]
LOC645904	chr22:22127982-22128041	0.441940165	0.282159047	2.182286412	0.320371214	4.937968039	0.058693174	0.248154139	0.023823843	PREDICTED: Homo sapiens similar to Mitotic spindle assembly checkpoint protein MAD1 (Mitotic arrest deficient-like protein 1) (MAD1-like 1) (Mitotic checkpoint MAD1 protein-homolog) (HsMAD1) (hMAD1) (Tax-binding protein 181) (LOC645904), mRNA [XM_928876]
NUSAP1	chr15:39455237-39455296	10.73924377	***2.41311E-06***	6.846925166	***5.84109E-05***	0.637561202	0.181184705	6.165005977	***1.39808E-08***	Homo sapiens nucleolar and spindle associated protein 1 (NUSAP1), transcript variant 1, mRNA [NM_016359]
PCNT	chr21:46607847-46607906	1.995536761	0.003603067	1.147115076	0.438068366	0.574840363	0.01131725	1.599365964	0.034052472	Homo sapiens pericentrin (kendrin) (PCNT), mRNA [NM_006031]
PCNT	chr21:46689818-46689877	2.13151517	0.009587076	1.535881154	0.029989851	0.720558397	0.164662802	1.74927465	0.025662446	Homo sapiens pericentrin (kendrin) (PCNT), mRNA [NM_006031]
PLK1	chr16:23608471-23608713	3.265872419	0.005250644	3.208935199	0.00025727	0.982566	0.956385248	7.3375786	0.000767782	Homo sapiens polo-like kinase 1 (Drosophila) (PLK1), mRNA [NM_005030]

Gene Name	Map Position	DvM Linear Ratio	DvM P- value	AvM Linear Ratio	AvM P value	AvD Linear Ratio	AvD P value	TvM Linear Ratio	TvM P value	Description
PLK1	chr16:23609129-23609188	4.787465478	0.000781001	4.08903615	0.000354447	0.854112927	0.630617439	7.443472158	***1.32082E-10***	Homo sapiens polo-like kinase 1 (Drosophila) (PLK1), mRNA [NM_005030]
PLK2	chr5:57785809-57785750	3.488306828	0.0244796	1.521062725	0.117594995	0.436046139	0.09118439	1.02254131	0.887469567	Homo sapiens polo-like kinase 2 (Drosophila) (PLK2), mRNA [NM_006622]
PLK3	chr1:44940687-44940747	2.435368737	0.109707642	1.201460306	0.558596682	0.49333815	0.195117292	1.620874084	0.069446961	Homo sapiens polo-like kinase 3 (Drosophila) (PLK3), mRNA [NM_004073]
PLK4	chr4:129164616-129164675	n/a	n/a	n/a	n/a	0.895450209	0.60614004	5.199779736	n/a	Homo sapiens polo-like kinase 4 (Drosophila) (PLK4), mRNA [NM_014264]
PLK4	chr4:129173787-129173846	11.32166634	***1.91662E-05***	8.767602137	***3.42365E-05***	0.774409161	0.478940104	15.54431987	0.046930589	Homo sapiens polo-like kinase 4 (Drosophila) (PLK4), mRNA [NM_014264]
SASS6	chr1:100261677-100261618	3.04994683	0.001368359	2.739787511	0.002069993	0.898306647	0.609683684	3.516256585	0.014796998	Homo sapiens spindle assembly 6 homolog (C. elegans) (SASS6), mRNA [NM_194292]
SERF1B	chr5:69356972-69357031	1.589652955	0.029834219	1.239638287	0.352283979	0.77981693	0.241576165	1.547922151	0.076344482	Homo sapiens small EDRK-rich factor 1B (centromeric) (SERF1B), mRNA [NM_022978]
SERF1B	chr5:69374401-69374460	1.023819803	0.875568098	1.236393913	0.280545039	1.207628441	0.318605991	1.296395013	0.212592082	Homo sapiens small EDRK-rich factor 1B (centromeric) (SERF1B), mRNA [NM_022978]
SFI1	chr22:30337566-30338661	1.145225859	0.606425131	0.765941736	0.25362742	0.66881282	0.062296319	1.616553871	0.182497052	Homo sapiens Sfi1 homolog, spindle assembly associated (yeast) (SFI1), transcript

Gene Name	Map Position	DvM Linear Ratio	DvM P- value	AvM Linear Ratio	AvM P value	AvD Linear Ratio	AvD P value	TvM Linear Ratio	TvM P value	Description
										variant 1, mRNA [NM_001007467] variant 1, mRNA [NM_001007467]
SFI1	chr22:30338984-30339043	0.969564121	0.927280494	0.667412121	0.167391802	0.688363056	0.179544473	1.708216391	0.109655104	Homo sapiens Sfi1 homolog, spindle assembly associated (yeast) (SFI1), transcript variant 1, mRNA [NM_001007467]
SMN2	chr5:69398703-69398921	2.137039469	0.030982119	1.90124909	0.023116142	0.88966494	0.699783579	0.783099838	0.422866214	Homo sapiens survival of motor neuron 2, centromeric (SMN2), transcript variant c, mRNA [NM_022877]
SPBC24	chr19:11118053-11117994	2.986090864	0.000543131	2.931432497	0.00578461	0.981695678	0.951721418	5.353491369	0.000107404	Homo sapiens spindle pole body component 24 homolog (S. cerevisiae) (SPBC24), mRNA [NM_182513]
SPBC25	chr2:169553522-169553463	16.74630849	***7.27785E-06***	9.383383693	0.000302853	0.560325501	0.227108378	11.85878736	***3.16569E-07***	Homo sapiens spindle pole body component 25 homolog (S. cerevisiae) (SPBC25), mRNA [NM_020675]
SYCE1	chr10:135259492-135259189	1.184337701	0.068071939	1.286719934	n/a	1.086446824	n/a	0.199583466	0.10467662	Homo sapiens synaptonemal complex central element protein 1 (SYCE1), transcript variant 2, mRNA [NM_201564]
THC2343415	chr4:124009351-124009292	2.143457766	0.043669847	1.49395673	0.206816648	0.696984449	0.332591864	0.574745619	n/a	Q5SUE1 (Q5SUE1) Centrin 4, partial (52%) [THC2343415]
76P	chr15:41483980-41484039	5.950048853	0.000136909	4.643172054	0.000223346	0.780358644	0.147011559	1.881091083	0.003462753	Homo sapiens gamma tubulin ring complex protein (76p gene) (76P), mRNA [NM_014444]

Environ Mol Mutagen. Author manuscript; available in PMC 2015 February 10.

Gene Name	Map Position	DvM Linear Ratio	DvM P- value	AvM Linear Ratio	AvM P value	AvD Linear Ratio	AvD P value	TvM Linear Ratio	TvM P value	Description
AA780798	chr6:030799960-030799901	1.978180771	0.002137747	1.591348	0.039743857	0.804450242	0.302976729	1.600971506	0.036356944	ag14d07.s1 Gessler Wilms tumor Homo sapiens cDNA clone IMAGE:1070317 3' similar to gb:J00314_rna2 TUBULIN BETA-1 CHAIN (HUMAN);, mRNA sequence [AA780798]
AI028577	chr2:132074237-132074178	0.679517636	0.181584774	1.115795872	0.570128513	1.642041079	0.100541347	0.854957638	0.834643704	AI028577 ow01h11.x1 Soares_testis_NHT Homo sapiens cDNA clone IMAGE:1645605 3' similar to gb:K00558 TUBULIN ALPHA-1 CHAIN (HUMAN);, mRNA sequence [AI028577]
AI608782	chr12:47808298-47808357	1.255935486	0.237944754	1.18596674	0.435074234	0.944289538	0.806340361	1.459355627	0.130521468	AI608782 tw94g05.x1 NCI_CGAP_HN6 Homo sapiens cDNA clone IMAGE:2267384 3' similar to gb:K00558 TUBULIN ALPHA-1 CHAIN (HUMAN);, mRNA sequence [AI608782]
AI911586	chr10:104492950-104492891	n/a	n/a	n/a	n/a	0.720982417	0.283031701	18.86056627	n/a	ty73h01.x1 NCI_CGAP_Kid11 Homo sapiens cDNA clone IMAGE:2284753 3' similar to SW:TTL_PIG P38160 TUBULIN--TYROSINE LIGASE ;, mRNA sequence [AI911586]

Gene Name	Map Position	DvM Linear Ratio	DvM P- value	AvM Linear Ratio	AvM P value	AvD Linear Ratio	AvD P value	TvM Linear Ratio	TvM P value	Description
AW168145	chr16:088529508-088529449	1.671060959	0.017452552	1.342976619	0.181410468	0.803667042	0.205957476	1.333594604	0.083987165	xg60e01.x1 NCI_CGAP_Ut4 Homo sapiens cDNA clone IMAGE:2632728 3' similar to gb:X00734_cds1 TUBULIN BETA-5 CHAIN (HUMAN);, mRNA sequence [AW168145]
BC014971	chr16:88690155-88690214	2.789518804	0.093886023	1.070134041	0.908832914	0.383626753	0.171254557	1.767978642	0.192001611	Homo sapiens, Similar to tubulin, beta, 2, clone IMAGE:4873024, mRNA. [BC014971]
H2-ALPHA	chr2:132071974-132072033	0.969319995	0.888268077	1.088894578	0.72631665	1.123359245	0.584331437	0.854448924	0.495356593	Homo sapiens alpha-tubulin isotype H2-alpha (H2-ALPHA), mRNA [NM_080386]
H2-ALPHA	chr2:132074162-132074221	1.105076099	0.604403333	0.963805346	0.83609939	0.872161969	0.250552949	0.734974792	0.104123911	Homo sapiens alpha-tubulin isotype H2-alpha (H2-ALPHA), mRNA [NM_080386]
K-ALPHA-1	chr12:47807959-47807900	0.857443642	0.560459713	1.185047241	0.604422153	1.382070125	0.325594025	1.174717108	0.580060146	Homo sapiens alpha tubulin (K-ALPHA-1), mRNA [NM_006082]
MGC16703	chr22:19688101-19688042	1.189996746	0.569120291	1.255005399	0.498103922	1.054629269	0.831504271	0.356314526	0.004960059	Homo sapiens alpha tubulin-like (MGC16703), mRNA [NM_145042]
TBCA	chr5:77023014-77022955	1.628337401	0.015750817	1.207337195	0.333723591	0.741453948	0.188358639	0.971893895	0.869550385	Homo sapiens tubulin-specific chaperone a (TBCA), mRNA [NM_004607]

Gene Name	Map Position	DvM Linear Ratio	DvM P- value	AvM Linear Ratio	AvM P value	AvD Linear Ratio	AvD P value	TvM Linear Ratio	TvM P value	Description
TBCC	chr6:42820720-42820661	0.995875905	0.985422176	1.589501306	0.126759341	1.596083707	0.084494378	1.176170582	0.527720869	Homo sapiens tubulin-specific chaperone c (TBCC), mRNA [NM_003192]
TBCC	chr6:42820889-42820830	1.003613754	0.984482864	1.67612549	0.063421457	1.670090195	0.031748746	1.041677783	0.878930352	Homo sapiens tubulin-specific chaperone c (TBCC), mRNA [NM_003192]
TBCD	chr17:78477601-78478354	1.488387681	0.214609459	1.723997872	0.019360207	1.158298939	0.627420613	1.226622933	0.495345392	Homo sapiens tubulin-specific chaperone d (TBCD), transcript variant 1, mRNA [NM_005993]
TBCD	chr17:78488452-78488511	1.399249127	0.175479398	1.213985031	0.173144039	0.86759749	0.56657747	1.748825524	0.007044583	Homo sapiens tubulin-specific chaperone d (TBCD), transcript variant 1, mRNA [NM_005993]
TBCD	chr17:78493800-78493859	1.19735066	0.409177942	1.044632883	0.775196054	0.872453591	0.565410914	2.334565662	0.001132949	Homo sapiens tubulin-specific chaperone d (TBCD), transcript variant 1, mRNA [NM_005993]
TBCE	chr1:231938185-231938244	1.70187682	0.008802425	1.923716165	0.000232169	1.130349825	0.468937133	1.674976767	0.003741768	Homo sapiens tubulin-specific chaperone e (TBCE), mRNA [NM_003193]
THC2307581	chr6:003169718-003169777	1.952910606	0.62434615	3.352015778	0.135931051	1.71642049	0.707633847	0.045570054	0.033095821	B25437 tubulin beta-2 chain - mouse (fragment) {Mus musculus;}, partial (18%) [THC2307581]
THC2307600	chr6:40075674-40075734	0.840555216	0.329703812	0.833605185	0.406911044	0.991731619	0.96364418	0.920517101	0.798113018	Q9JJY6 (Q9JJY6) Beta-tubulin (Fragment), partial (46%) [THC2307600]
TTBK2	chr15:40825647-40825588	0.775213323	0.265200427	1.243886247	0.349996464	1.604572844	0.024574108	0.710953596	0.31385279	Homo sapiens tau tubulin kinase 2 (TTBK2), mRNA [NM_173500]

Gene Name	Map Position	DvM Linear Ratio	DvM P- value	AvM Linear Ratio	AvM P value	AvD Linear Ratio	AvD P value	TvM Linear Ratio	TvM P value	Description
TTBK2	chr15:40856649-40856590	2.339489963	0.047526696	2.276855802	0.044370793	0.973227429	0.935856907	0.884497395	0.622843256	Homo sapiens tau tubulin kinase 2 (TTBK2), mRNA [NM_173500]
TTL	chr2:112968040-112968099	6.663981858	0.000240118	3.010395864	0.002774944	0.451741305	0.003176487	1.511421614	0.1010284	Homo sapiens tubulin tyrosine ligase (TTL), mRNA [NM_153712]
TTL	chr2:112976906-112976965	14.4020585	***2.891E-05***	5.296386338	***4.9465E-05***	0.367752036	0.010429262	3.343359036	0.239889706	Homo sapiens tubulin tyrosine ligase (TTL), mRNA [NM_153712]
TTL	chr2:113002674-113002733	5.408645901	0.000358103	2.956077359	0.005525021	0.546546661	0.044370259	1.848052212	0.001789355	Homo sapiens tubulin tyrosine ligase (TTL), mRNA [NM_153712]
TTLL1	chr22:41772389-41772330	2.455246928	0.004617839	1.608578367	0.082121147	0.655159507	0.044975404	1.001655349	0.995238055	Homo sapiens tubulin tyrosine ligase-like family, member 1 (TTLL1), transcript variant 2, mRNA [NM_001008572]
TTLL10	chr1:1160312-1160371	n/a	n/a	n/a	n/a	1.326906974	n/a	2.978726245	n/a	Homo sapiens tubulin tyrosine ligase-like family, member 10 (TTLL10), mRNA [NM_153254]
TTLL11	chr9:121831419-121831360	0.698405365	0.182417357	0.630991229	0.048646634	0.903474202	0.729798999	0.647220855	0.120318237	Homo sapiens tubulin tyrosine ligase-like family, member 11 (TTLL11), mRNA [NM_194252]
TTLL12	chr22:41887399-41887340	2.138427795	0.0014636	1.858673953	0.00429454	0.869177794	0.386698421	2.855889328	0.000450266	Homo sapiens tubulin tyrosine ligase-like family, member 12 (TTLL12), mRNA [NM_015140]
TTLL2	chr6:167725671-167725730	n/a	n/a	n/a	n/a	n/a	n/a	1.628620287	n/a	Homo sapiens tubulin tyrosine ligase-like family, member 2

Gene Name	Map Position	DvM Linear Ratio	DvM P- value	AvM Linear Ratio	AvM P value	AvD Linear Ratio	AvD P value	TvM Linear Ratio	TvM P value	Description
										(TTLL2), mRNA [NM_031949] (TTLL2), mRNA [NM_031949]
TTLL3	chr3:9843876-9843935	0.344169157	0.001825435	0.292954647	0.000801308	0.851193782	0.304955949	0.485375458	0.008726558	Homo sapiens tubulin tyrosine ligase-like family, member 3, mRNA (cDNA clone IMAGE:3841498), complete cds. [BC009479]
TTLL3	chr3:9851825-9851884	1.065101337	0.676523871	0.774999999	0.101099692	0.727630294	0.071154571	2.437055254	0.000714055	Homo sapiens tubulin tyrosine ligase-like family, member 3 (TTLL3), transcript variant 2, mRNA [NM_015644]
TTLL3	chr3:9852427-9852486	0.731172239	0.19043441	0.805874282	0.309120618	1.102167505	0.638033707	2.514457619	0.006736965	Homo sapiens tubulin tyrosine ligase-like family, member 3 (TTLL3), transcript variant 2, mRNA [NM_015644]
TTLL4	chr2:219443837-219443896	2.550471097	0.000415031	3.571844465	***2.43491E-05***	1.400464592	0.009065142	3.094473776	0.006425222	Homo sapiens tubulin tyrosine ligase-like family, member 4 (TTLL4), mRNA [NM_014640]
TTLL5	chr14:75399792-75399851	1.155370394	0.596550761	1.824202391	0.001201405	1.57888968	0.139034148	2.380077506	***9.96478E-08***	Homo sapiens tubulin tyrosine ligase-like family, member 5 (TTLL5), mRNA [NM_015072]
TTLL6	chr17:44195237-44195178	0.43520045	0.150939071	0.827230613	0.77291541	1.90080367	0.235451172	0.342220962	0.299756463	Homo sapiens tubulin tyrosine ligase-like family, member 6 (TTLL6), mRNA [NM_173623]
TTLL6	chr17:44217418-44217359	0.608140153	n/a	0.746786542	n/a	1.22798427	n/a	0.611001865	0.653278394	Homo sapiens tubulin tyrosine ligase-like family, member 6 (TTLL6), mRNA [NM_173623]

Gene Name	Map Position	DvM Linear Ratio	DvM P- value	AvM Linear Ratio	AvM P value	AvD Linear Ratio	AvD P value	TvM Linear Ratio	TvM P value	Description
TTLL7	chr1:84068058-84060815	1.648672303	0.354687912	0.519839499	0.288668436	0.315307959	0.112306095	0.080480022	***3.35687E-05***	Homo sapiens tubulin tyrosine ligase-like family, member 7 (TTLL7), mRNA [NM_024686]
TTLL7	chr1:84081836-84068180	1.310065691	0.611118581	0.964126748	0.964425663	0.735937712	0.727708411	0.027896848	***3.02846E-07***	Homo sapiens tubulin tyrosine ligase-like family, member 7 (TTLL7), mRNA [NM_024686]
TUBA1	chr2:219940634-219940575	0.572675993	0.087416476	1.104193813	0.805321055	1.928130087	0.164332075	2.126422654	0.008900223	Homo sapiens tubulin, alpha 1 (testis specific) (TUBA1), mRNA [NM_006000]
TUBA1	chr2:219940711-219940652	0.687745013	0.202200336	1.269904259	0.540851238	1.846475417	0.183063653	1.951896463	0.017287701	Homo sapiens tubulin, alpha 1 (testis specific) (TUBA1), mRNA [NM_006000]
TUBA1	chr2:219940759-219940700	0.750639634	0.102679812	1.081207133	0.734460844	1.440381088	0.137420149	1.152073381	0.54717231	Homo sapiens tubulin, alpha 1 (testis specific) (TUBA1), mRNA [NM_006000]
TUBA1	chr2:219941227-219941168	0.849512285	0.379802777	1.298166666	0.33820833	1.528131717	0.162818869	1.760373391	0.020135594	Homo sapiens tubulin, alpha 1 (testis specific) (TUBA1), mRNA [NM_006000]
TUBA2	chr13:18649197-18649138	1.119600211	0.626472071	1.816294981	0.047888997	1.622271024	0.162113969	2.514239847	0.010244898	Homo sapiens tubulin, alpha 2 (TUBA2), transcript variant 2, mRNA [NM_079836]
TUBA3	chr12:47865739-47865680	0.939133616	0.821975246	1.160677517	0.585287238	1.235902428	0.460677371	0.845469497	0.506095413	Homo sapiens tubulin, alpha 3 (TUBA3), mRNA [NM_006009]
TUBA6	chr12:47949701-47949900	1.13867431	0.670390308	1.458724134	0.175768655	1.281072314	0.425448758	0.896282829	0.679542622	Homo sapiens tubulin, alpha 6 (TUBA6), mRNA [NM_032704]

Gene Name	Map Position	DvM Linear Ratio	DvM P- value	AvM Linear Ratio	AvM P value	AvD Linear Ratio	AvD P value	TvM Linear Ratio	TvM P value	Description
TUBA6	chr12:47952552-47952611	1.439720094	0.184643278	1.671964313	0.051572976	1.161312063	0.593785586	1.146649828	0.511143061	Homo sapiens tubulin, alpha 6 (TUBA6), mRNA [NM_032704]
TUBA6	chr12:47953065-47953124	1.096186884	0.659628265	1.364777204	0.187923114	1.245022381	0.426930697	1.263565105	0.298454674	Homo sapiens tubulin, alpha 6 (TUBA6), mRNA [NM_032704]
TUBA6	chr12:47953297-47953356	2.519503536	0.004459479	2.463328773	0.00149327	0.977704035	0.931823772	2.773231793	0.000728057	Homo sapiens tubulin, alpha 6 (TUBA6), mRNA [NM_032704]
TUBA8	chr22:16988374-16988433	1.004108425	0.989047759	0.953525457	0.80109154	0.949623998	0.856962984	1.167233958	0.393680863	Homo sapiens tubulin, alpha 8 (TUBA8), mRNA [NM_018943]
TUBAL3	chr10:5425268-5425209	0.204902439	0.255851845	0.994791897	0.996853074	4.854953908	0.030404166	1.092128748	0.947104434	Homo sapiens tubulin, alpha-like 3 (TUBAL3), mRNA [NM_024803]
TUBB	chr6:30799847-30799906	1.584278885	0.00566468	1.372285719	0.184164808	0.866189489	0.517774048	1.524299646	0.04644169	Homo sapiens tubulin, beta (TUBB), mRNA [NM_178014]
TUBB	chr6:30799884-30799943	1.492109899	0.079513857	1.244767024	0.453531673	0.834232804	0.493657273	1.234137979	0.376482678	Homo sapiens tubulin, beta (TUBB), mRNA [NM_178014]
TUBB	chr6:30800501-30800560	1.584623411	0.107036108	1.554573084	0.12797646	0.981036297	0.947810448	1.767278199	0.074347725	Homo sapiens tubulin, beta (TUBB), mRNA [NM_178014]
TUBB1	chr20:57033076-57033135	1.283709237	n/a	n/a	n/a	n/a	n/a	0.560774764	n/a	Homo sapiens tubulin, beta 1 (TUBB1), mRNA [NM_030773]
TUBB1	chr20:57034639-57034698	n/a	n/a	n/a	n/a	0.623141934	n/a	1.150878305	n/a	Homo sapiens tubulin, beta 1 (TUBB1), mRNA [NM_030773]
TUBB2A	chr6:3099093-3099034	0.515399738	0.128243869	0.223915793	0.001080418	0.434450731	0.106193622	0.225151386	0.000305294	Homo sapiens tubulin, beta 2A (TUBB2A), mRNA [NM_001069]

Gene Name	Map Position	DvM Linear Ratio	DvM P- value	AvM Linear Ratio	AvM P value	AvD Linear Ratio	AvD P value	TvM Linear Ratio	TvM P value	Description
TUBB2A	chr6:3099458-3099399	0.953497535	0.865848881	0.569640111	0.099851658	0.597421692	0.168494941	0.428657284	0.006462263	Homo sapiens tubulin, beta 2A (TUBB2A), mRNA [NM_001069]
TUBB2B	chr6:3169809-3169750	0.275439519	0.163388644	0.286915192	0.040654721	1.041663132	0.964822468	0.019668205	***1.90633E-07***	Homo sapiens tubulin, beta 2B (TUBB2B), mRNA [NM_178012]
TUBB2C	chr9:137413483-137413542	1.756253855	0.028564242	1.582950165	0.036152087	0.901321959	0.686052399	2.291435797	0.004324287	Homo sapiens tubulin, beta 2C (TUBB2C), mRNA [NM_006088]
TUBB2C	chr9:137413938-137413996	1.254805703	0.383709045	1.297507044	0.227619348	1.034030241	0.901015552	2.08304547	0.014414019	Homo sapiens tubulin, beta 2C (TUBB2C), mRNA [NM_006088]
TUBB3	chr16:88529436-88529495	1.400627824	0.01905224	1.051885025	0.818812703	0.751009659	0.236299682	1.236941281	0.121543798	Homo sapiens tubulin, beta 3 (TUBB3), mRNA [NM_006086]
TUBB3	chr16:88529938-88529997	3.034430862	0.008413314	1.200762639	0.641393838	0.395712637	0.056793328	1.056767975	0.804078784	Homo sapiens tubulin, beta 3 (TUBB3), mRNA [NM_006086]
TUBB4	chr19:6445704-6445645	1.53070267	0.03149165	1.34635951	0.050495638	0.879569584	0.42965393	0.66604622	0.095386797	Homo sapiens tubulin, beta 4 (TUBB4), mRNA [NM_006087]
TUBB4	chr19:6446948-6446889	0.863357155	0.673930756	0.374835762	0.032436531	0.434160717	0.068039613	0.168094436	0.001095858	Homo sapiens tubulin, beta 4 (TUBB4), mRNA [NM_006087]
TUBB6	chr18:12315997-12316056	1.0407388	0.734339924	0.787111865	0.266446156	0.756301067	0.182486723	0.686841947	0.109123548	Homo sapiens tubulin, beta 6 (TUBB6), mRNA [NM_032525]
TUBB6	chr18:12316476-12316535	0.178899863	0.152612007	0.033417784	0.000983938	0.18679603	0.200910155	0.115261559	0.000208772	Homo sapiens tubulin, beta 6 (TUBB6), mRNA [NM_032525]
TUBB8	chr10:83404-83345	1.324871811	0.14689598	1.033948749	0.870229955	0.780414181	0.341973178	1.059355311	0.706490087	Homo sapiens tubulin, beta 8 (TUBB8), mRNA [NM_177987]
TUBD1	chr17:55292536-55292477	0.813032587	0.606588421	1.079556477	0.80028366	1.327814524	0.380245482	0.75772502	0.315577512	Homo sapiens tubulin, delta 1

Gene Name	Map Position	DvM Linear Ratio	DvM P- value	AvM Linear Ratio	AvM P value	AvD Linear Ratio	AvD P value	TvM Linear Ratio	TvM P value	Description
										(TUBD1), mRNA [NM_016261] (TUBD1), mRNA [NM_016261]
TUBE1	chr6:112502698-112502639	5.282486849	0.000264413	2.52173674	0.005352034	0.477376814	0.016883159	0.789883777	0.127356069	Homo sapiens tubulin, epsilon 1 (TUBE1), mRNA [NM_016262]
TUBG1	chr17:38018548-38018607	1.981144469	0.058338359	2.052718766	0.000182858	1.036127752	0.903060784	1.300489191	0.368611715	Homo sapiens tubulin, gamma 1 (TUBG1), mRNA [NM_001070]
TUBG2	chr17:38069000-38071031	1.677095651	0.074754047	1.651259413	0.000681646	0.984594654	0.948279178	1.161587557	0.597912576	Homo sapiens tubulin, gamma 2 (TUBG2), mRNA [NM_016437]
TUBGCP2	chr10:134986328-134986269	1.218542935	0.204636766	1.353312879	0.010136853	1.110599257	0.519396123	1.069323142	0.739996284	Homo sapiens tubulin, gamma complex associated protein 2 (TUBGCP2), mRNA [NM_006659]
TUBGCP3	chr13:112188148-112188089	1.873083313	0.011437334	1.775375299	0.023289891	0.947835735	0.835335934	2.393651106	0.002363706	Homo sapiens tubulin, gamma complex associated protein 3 (TUBGCP3), mRNA [NM_006322]
TUBGCP3	chr13:112188401-112188342	2.13005795	0.043459515	1.948168191	0.009516649	0.91460807	0.793708237	2.478424836	0.000169652	Homo sapiens tubulin, gamma complex associated protein 3 (TUBGCP3), mRNA [NM_006322]
TUBGCP3	chr13:112206955-112206434	4.316434459	0.002124934	4.104401538	***1.76066E-06***	0.950877762	0.859372307	1.843666311	0.048125256	Homo sapiens tubulin, gamma complex associated protein 3 (TUBGCP3), mRNA [NM_006322]
TUBGCP5	chr15:20420386-20421393	2.190443907	0.016181992	2.373349141	0.011563644	1.083501446	0.557521077	1.677043363	0.144830062	Homo sapiens tubulin, gamma complex associated protein 5 (TUBGCP5),

Gene Name	Map Position	DvM Linear Ratio	DvM P- value	AvM Linear Ratio	AvM P value	AvD Linear Ratio	AvD P value	TvM Linear Ratio	TvM P value	Description
										mRNA [NM_052903] mRNA [NM_052903]
TUBGCP6	chr22:48959229-48959170	1.094052854	0.361173466	0.717879194	0.02461539	0.656165003	0.003882231	1.220462294	0.199609257	Homo sapiens tubulin, gamma complex associated protein 6 (TUBGCP6), transcript variant 2, mRNA [NM_001008658]